Coverage, Capacity, and Energy Efficiency Analysis in the Uplink of mmWave Cellular Networks

Oluwakayode Onireti, *Member, IEEE*, Ali Imran, *Member, IEEE*, and Muhammad Ali Imran, *Senior Member, IEEE*

***Abstract*—In this paper, using the concept of stochastic geometry, we present an analytical framework to evaluate the signal-to-interference-and-noise-ratio (SINR) coverage in the uplink of millimeter wave cellular networks. By using a distance-dependent line-of-sight (LOS) probability function, the location of LOS and nonLOS users are modeled as two independent nonhomogeneous Poisson point processes, with each having a different pathloss exponent. The analysis takes account of per-user fractional power control (FPC), which couples the transmission of users based on location-dependent channel inversion. We consider the following scenarios in our analysis: 1) pathloss-based FPC (PL-FPC) which is performed using the measured pathloss and 2) distance-based FPC (D-FPC) which is performed using the measured distance. Using the developed framework, we derive expressions for the area spectral efficiency and energy efficiency. Results suggest that in terms of SINR coverage, D-FPC outperforms PL-FPC scheme at high SINR where the future networks are expected to operate. It achieves equal or better area spectral efficiency and energy efficiency compared with the PL-FPC scheme. Contrary to the conventional ultra-high frequency cellular networks, in both FPC schemes, the SINR coverage decreases as the cell density becomes greater than a threshold, while the area spectral efficiency experiences a slow growth region.**

***Index Terms*—5G cellular network, fractional power control, millimeter wave, stochastic geometry, uplink.**

I. Introduction

INCREASED bandwidth by moving into the millimeter wave (mmWave) band is one of the primary approaches toward meeting the data rate requirement of the fifth generation (5G) cellular networks [1]–[3]. According to [3], the available spectrum for cellular communications at the mmWave band can be easily 200 times greater than the spectrum presently allocated for that purpose below the 3 GHz. The mmWave band ranging from 30-300 GHz has already been considered for wireless services such as fixed access and personal area networking [4], [5]. However, such frequency bands have long been deemed unsuitable for cellular communications as a result of the large free space pathloss and poor penetration (i.e., blockage effect) through materials such as water, concrete, etc. Only recently did survey measurements and capacity studies of mmWave technology reveal its promise for urban small cell deployments [2], [6]–[8].

In addition to the huge available bandwidth in the mmWave band, the smaller wavelength associated with the band combined with recent advances in low-power CMOS RF circuits have paved the way for the use of more miniaturized antennas at the same physical area of the transmitter and receiver to provide array gain [3], [8]. With such a large antenna array, the mmWave cellular system can apply beamforming at the transmit and receive sides to provide array gain which compensates for the near-field pathloss [9]. For illustration purpose, given a fixed antenna area, a beam at 30 GHz will have about 20 dB more gain than a beam at 3 GHz, and from Friss's law, signals at the former also experience 20 dB larger pathloss than signals at the latter [10]. Hence, array gain can be used to counter the effect of the larger pathloss associated with the mmWave band.

A major challenge in the mmWave band is its extreme sensitivity to the propagation environment. As a result of the blockage effect associated with mmWave, outdoor mmWave base stations (BSs) are more likely to serve outdoor users [11]. Furthermore, it has been revealed via the channel measurements in [2], [6] that blockages result in a significant difference between the line-of-sight (LOS) and non-line-of-sight (NLOS) pathloss characteristics. The measurements showed that mmWave signals propagate with a pathloss exponent of 2 in LOS paths and a much higher pathloss exponent with additional shadowing in NLOS paths [2], [6]. Furthermore, the NLOS pathloss exponent tends to be more dependent on the scattering environment [12], with typical measured values ranging from 3.2 to 5.8 [2], [6]. In order to maintain connectivity when the LOS path between the transmitter and the receiver in a mmWave network is blocked, the authors in [13] exploited the reflected NLOS links by jointly optimizing relay and link selection for the transmitter-receiver pair. In addition, the authors in [14] proposed a multiband directional network discovery scheme to address the network discovery problem in mmWave networks.

Regarding vehicular technology, mmWave is very attractive for intra-vehicle communications due to its inability to easily penetrate and interfere with other vehicular networks (due to high vehicle penetration losses). The use of mmWave

Manuscript received June 20, 2017; revised September 26, 2017; accepted November 1, 2017. Date of publication December 8, 2017; date of current version May 14, 2018. This work was supported in part by the DARE project through the Engineering and Physical Sciences Research Council U.K. Global Challenges Research Fund Allocation under Grant EP/P028764/1 and in part by the National Science Foundation under Grant 1730650, Grant 1718956, and Grant 1559483. The review of this paper was coordinated by Dr. Z. Ding. *(Corresponding author: Oluwakayode Onireti.)*

O. Onireti and M. A. Imran are with the School of Engineering, University of Glasgow, Glasgow, G12 8QQ, U.K. (e-mail: Oluwakayode.Onireti@glasgow.ac.uk; Muhammad.Imran@glasgow.ac.uk).

A. Imran is with the School of Electrical and Computer Engineering, University of Oklahoma, Tulsa, OK 74135 USA (e-mail: ali.imran@ou.edu).

Color versions of one or more of the figures in this paper are available online at http://ieeexplore.ieee.org.

Digital Object Identifier 10.1109/TVT.2017.2775520

transmission at 24 and 77 GHz for automotive radar and cruise control makes it foreseeable that mmWave will find its way into other vehicular applications in the coming years [15].

A. Related Work on Stochastic Geometry Framework for mmWave Cellular Networks

Recently, use of stochastic geometry-based analysis was proposed to assess the capacity of conventional UHF cellular systems in [16]–[21]. Focusing on the downlink channel of conventional UHF cellular networks, the authors in [16] modeled the BS location as a Poisson point process (PPP) on the plane, and derived the signal-to-interference-and-noise-ratio (SINR) coverage probability and the average rate of a typical user. Moreover, according to [16], modeling BSs as PPP provides lower bounds to the coverage probability of real deployment. An extension of the stochastic model to the uplink channel of UHF cellular networks, which is based on the dependence assumption where user and BS point processes are such that each BS serves a single user in a given resource block, was presented in [17]. The authors in [17] also included a per-user fractional power control (FPC) scheme in their model. The results in [16] have also been extended to multi-tier UHF cellular networks in [18]–[21] and for systems performance analysis in [22]–[24]. However, as a result of the blockage effect and the different propagation model, the results obtained for UHF networks are not applicable to mmWave networks.

In order to analyze the system performance in mmWave networks, a stochastic blockage model, where the blockage parameters are characterized by some random distributions, was presented for such network in [25]. Also using the stochastic blockage process, authors in [12] proposed a framework to analyze the SINR and rate coverage probability in the downlink of mmWave networks while considering outdoor mmWave BSs and outdoor users. In [26], [27], a multi-slope pathloss model (where different distance ranges are subjected to different pathloss exponent), which is applicable for the mmWave model was presented for the downlink channel. In [28], a more comprehensive analytical framework for mmWave networks, which further incorporates self-backhauling but with a simplified blockage model was presented.

B. Contributions and Organization

While downlink performance of mmWave based networks has been investigated in several recent studies as discussed above, to the best of authors knowledge, this is the first study to investigate coverage, area spectral efficiency, and energy efficiency for uplink of mmWave cellular networks, and compare their performance with UHF based networks. The contributions and organization of this paper can be summarized as follows:

- We present a stochastic geometry framework for evaluating the SINR coverage in the uplink of mmWave cellular networks. Two factors that make the uplink coverage analysis for mmWave distinct from that of UHF are: a) User battery consumption becomes a major constraint because of wide bandwidth and increased losses. b) Compared to mmWave BSs, users are likely to have coarser beamforming, thus making interference in uplink more challenging. To address these challenges, in our analysis we incorporate the per-user FPC. The aim of the FPC scheme is to minimize mobile (user) battery consumption and minimize interference to other cells. Here we consider two FPC schemes: i) Pathloss-based FPC (PL-FPC), which is the conventional approach and is based on the measured pathloss and ii) Distance-based FPC (D-FPC), which is based on the measured distance.
- We present a detailed system model for the uplink of mmWave networks and review the expressions of the distribution of the distance between a typical user and its serving BS, which serves as a basis for our own derivation. We model the location of users and BSs as realizations of the PPP. Similar to [12] that is focused on the downlink, we introduce the blockage effect by modeling the probability that a link is LOS as a function of the link length. We then model the transmit power of the users based on the two FPC schemes (Section II).
- Based on the proposed modeling, it occurs that the random variables denoting the distance between each user and its serving BS (LOS or NLOS) are identically distributed but not independent in general. Hence, we prove that this dependence is weak and can, therefore, be ignored for analytical tractability (Section II).
- Building on the independence assumption, we present a formal proof of the SINR coverage probability for both PL-FPC and D-FPC. Afterwards, we derive the SINR coverage probability expressions for the case with a) fixed transmit power, i.e., no power control, b) simplified LOS probability function and c) the noise-limited scenario (Section III). Numerical results show the accuracy of our approximations for a wide range of SINR thresholds and BS densities.
- Using the developed framework in Section III, we derive the area spectral efficiency, the energy efficiency and rate fairness expressions in the uplink of mmWave cellular networks (Section IV).
- Leveraging on the derived analytical expressions and extensive Monte-Carlo simulations, we present a detailed numerical analysis that compares the performance of mmWave networks with that of UHF based networks and shows following new insights (Section V):

1) Despite the correlation between the distance of interfering users, a simplified model that assumes the distance of inferring users to be independent can yield highly accurate coverage results, for high BS densities. As high BS densities are intrinsic to mmWave networks, the presented analysis provides an accurate model for estimating uplink coverage probability.
2) Contrary to the common belief that mmWave networks can be modeled as noise-limited networks, our uplink analysis shows that SNR coverage probability tracks the SINR coverage probability for a threshold low BS densities up to $10^{-1.8}$ BSs/km^2. However, for larger BS densities, the interference dominates and a gap between the SINR and SNR coverage emerges.

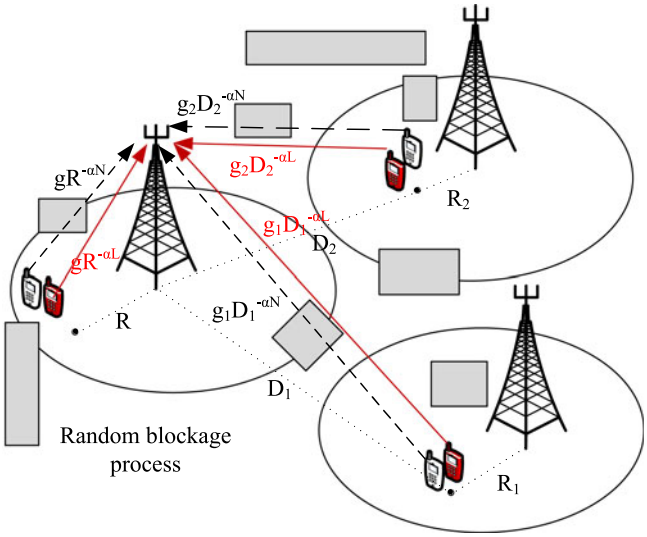

Fig. 1. Visual representation of the uplink of mmWave cellular networks, focusing on the served user and two interfering users in adjacent cells. Blockages are modeled as random process of rectangles as in [12]. White and red color marked user denotes the LOS and NLOS representation of the same user.

3) The D-FPC scheme gives better or equivalent performance compared with the PL-FPC scheme in terms of the area spectral efficiency and energy efficiency. On the other hand, the PL-FPC scheme achieves comparatively a higher fairness index.
4) Contrary to UHF cellular networks, the area spectral efficiency in mmWave cellular networks suffers a slow growth region as the BS density increases.

The key findings of the paper are concluded in Section VI. A preliminary version of this work has been reported in [29]. Herein, we have presented the SINR coverage probability with simplified LOS probability function. Furthermore, the area spectral efficiency, energy efficiency and fairness index expressions have been derived.

II. System Model and Assumptions

A. Network Model

We consider the uplink of a mmWave cellular network and focus on the SINR coverage experienced by outdoor users served by outdoor BSs. Fig. 1 gives a visual representation of the uplink system model. The outdoor BSs are spatially distributed in $\mathbb{R}^2$ according to an independent homogeneous PPP with density λ. The user locations (before association) are assumed to form a realization of homogeneous PPP with density λ_u. Each BS serves a single user per channel, which is randomly selected from all the users located in its Voronoi cell by using a round-robin scheduler. Hence, the user PPP λ_u is thinned to obtain a point process $\Phi = \{X_z\}$, where X_z is the location active outdoor users. As in [20], [30], we assume that the active users also form PPP even after associating just one user per BS. Since we have one active user per cell, the density ϕ of the thinned PPP of active users is set to be equal to the BS density λ. Table I summarizes all the notations used throughout the paper.

TABLE I
Summary of Notation

Notation	Description
λ	BS density
λ_u	User density
Φ, $\phi = \lambda$	Active user PPP, active user density
Φ_L, Φ_N	PPP of LOS user, PPP of NLOS user
$p(R)$	Probability that a link of length R is LOS
β	Blockage parameter
$L(R)$	Path loss at distance R
R_L (R_N)	Distance of LOS(NLOS) typical user to the reference BS
$\mathcal{F}_{R_L}$	PDF of the distance R_L between a LOS typical user and the reference BS
$\mathcal{F}_{R_N}$	PDF of the distance R_N between a NLOS typical user and the reference BS
C_b	Path loss at the 1 m where $b \in$ {LOS, NLOS}
α_b	Path loss exponent where $b \in$ {LOS, NLOS}
$\mathcal{Z}$	Set of interfering users
D_z	Distance of an interfering user to the reference BS
R_z	Distance of an interfering user to its serving BS
$\mathcal{F}_{R_{z,L}}$	PDF of the distance R_z when the link is LOS
$\mathcal{F}_{R_{z,N}}$	PDF of the distance R_z when the link is NLOS
$G_s(\theta_s)$	Antenna gain pattern as a function of angle θ_s about the steering angle where $s \in$ {UE, BS}
κ_s, $G_s^{\max}$	Beamwidth, main lobe gain
$G_s^{\min}$	and side lobe gain where $s \in$ {UE, BS}
G_l	Total directivity gain in the lth link
θ_u^1, θ_b^1	lth interference link user's boresite angle and angle of arrival at reference BS
(a_k, b_k)	PMF parameter of the random variable G_l, b_k is the probability that $G_l = a_k$ for $k \in \{1, 2, 3, 4\}$
N_b	Nakagami fading parameter where $b \in$ {LOS,NLOS}
g_l	Small-scale fading of the lth link
τ	Power control factor
P_b^0	User or network specific parameter related to the target mean received power where $b \in$ {LOS, NLOS}
σ^2	Noise power
B	Total bandwidth
Υ	Achievable data rate
$\mathcal{S}$	Area spectral efficiency
$\mathcal{R}$	Average ergodic spectral efficiency
$\mathcal{A}_b$	The association probability of typical user for $b \in$ {LOS, NLOS}
$P_c(\Gamma)$	The coverage probability at SINR Γ, $P_c(\Gamma) \mathbb{P}(\text{SINR} > \Gamma)$
$P_{c,b}(\Gamma)$	The conditional coverage probability given the BS served a user in Φ_b where $b \in$ {LOS, NLOS}
R_B	Size of LOS disc
$\mathcal{E}_{\text{eff}}$	Energy efficiency
$\mathcal{P}_{\text{tot}}$	Average uplink power consumption
P_c	User circuit power
P_u	Power consumed by BS for uplink processing
$\mathcal{P}$	average transmit power of user in Φ_b
$\mathcal{J}$	Jain's fairness

We perform our analysis on the typical outdoor user whose connected BS is termed as the reference BS. As a result of the blockage process, whose distribution is stationary and isotropic, the reference BS is either LOS or NLOS to the typical user. Here we say that a typical user at the origin O is LOS to the BS at E if and only if there is no blockage intersecting the link OE. Due to the presence of blockage, only a subset of the outdoor users Φ is in LOS with their tagged BS. Let Φ_L be the point process of the LOS users, and $\Phi_N = \Phi / \Phi_L$ be the process of NLOS users. We define the LOS probability function $p(R)$ as the probability that a link of length R is LOS. Note that the

function $p(R)$ depends only on the length of the link R and that it is a non-increasing function of R, such that the longer the link the more likely that it will be intersected by blockage(s) [12]. The NLOS probability of the link is thus $1-p(R)$. The LOS probability function is modeled from a stochastic blockage model, where the blockage is modeled as a rectangle Boolean scheme. $p(R)=e^{-\beta R}$, where β is a parameter determined by the average size and the density of the blockages [25]. Different pathloss models are applied to the LOS and NLOS links. Hence, given a link with length R, its pathloss gain $L(R)$ is computed as

$$L(R)=\mathbb{I}\left(p\left(R\right)\right)C_L R^{-\alpha_L}+\left(1-\mathbb{I}\left(p\left(R\right)\right)\right)C_N R^{-\alpha_N}, \quad (1)$$

where $\mathbb{I}(r)$ is a Bernoulli random variable with parameter r, C_L and C_N are the intercepts on the LOS and NLOS pathloss expressions, α_L and α_N are the LOS and NLOS pathloss exponents. We assume that a user, either LOS or NLOS, associates with the BS that offers the maximum long-term averaged received power, i.e., the effect of fading is averaged out and hence ignored.[1]

B. Independent LOS Probability

Without loss of accuracy, we ignore the correlation of the blockage effects between the links as demonstrated in [25] and assume that the LOS probabilities are independent between links. Consequently, the LOS user process Φ_L and the NLOS process Φ_N form two independent non-homogeneous PPPs with density functions $\lambda p(R)$ and $\lambda(1-p(R))$, respectively, where R is the Euclidean distance between a sender and receiver. Following the independence of the LOS probability, the distributions of the distance between the reference BS and, a LOS or NLOS typical user are given next.

Distribution of the distance R_L between the reference BS and a LOS user: Given that the typical user has a LOS association with the reference BS, the probability distribution function of the distance R_L between the typical user and reference BS can be expressed from (6) in [12] as

$$\mathcal{F}_{R_L}(r)=\frac{2\pi\lambda r e^{-\beta r}}{\mathcal{A}_L}e^{\left(-2\pi\lambda\left(\frac{(\beta q_l r^{v_l}+1)}{\beta^2 e^{\beta q_l r^{v_l}}}-\frac{(\beta r+1)}{\beta^2 e^{\beta r}}+\frac{q_l^2 r^{2v_l}}{2}\right)\right)} \quad (2)$$

after expansion, where $q_l=(C_N/C_L)^{\frac{1}{\alpha_N}}$, $v_l=\alpha_L/\alpha_N$ and

$$\mathcal{A}_L=2\pi\lambda\int_0^\infty re^{-\beta r}e^{\left(-2\pi\lambda\left(\frac{(\beta q_l r^{v_l}+1)}{\beta^2 e^{\beta q_l r^{v_l}}}-\frac{(\beta r+1)}{\beta^2 e^{\beta r}}+\frac{q_l^2 r^{2v_l}}{2}\right)\right)}\mathrm{d}r \quad (3)$$

is the probability that the reference BS is connected to a LOS user.

Distribution of the distance R_N between the reference BS and a NLOS user: Given that the typical user has a NLOS association with the reference BS, the probability distribution function of the distance R_N between the typical user and the reference BS can be expressed from (7) in [12] as

$$\mathcal{F}_{R_N}(r)=\frac{2\pi\lambda r\left(1-e^{-\beta r}\right)}{\mathcal{A}_N}e^{\left(-2\pi\lambda\left(\frac{(\beta r+1)}{\beta^2 e^{\beta r}}-\frac{(\beta q_n r^{v_n}+1)}{\beta^2 e^{\beta q_n r^{v_n}}}+\frac{r^2}{2}\right)\right)} \quad (4)$$

after expansion, where $q_n=(C_L/C_N)^{\frac{1}{\alpha_L}}$, $v_l=\alpha_N/\alpha_L$ and

$$\mathcal{A}_N=1-\mathcal{A}_L \quad (5)$$

is the probability that the reference BS is connected to a NLOS user.

C. Antenna Gain Pattern and Directivity

For tractability of analysis, all users and mmWave BSs are equipped with directional antennas with sectored gain pattern [28]. The antenna gain pattern for a BS as a function of the angle off its boresight direction θ_b is given by

$$G_b(\theta_b)=\begin{cases}G_b^{\max} & \text{if } |\theta_b|\le\kappa_b\\ G_b^{\min} & \text{otherwise}\end{cases}, \quad (6)$$

where κ_b is the beamwidth of the BS antenna. The user antenna gain pattern $G_u(\theta_u)$ is modeled in a similar manner such that

$$G_u(\theta_u)=\begin{cases}G_u^{\max} & \text{if } |\theta_u|\le\kappa_u\\ G_u^{\min} & \text{otherwise}\end{cases}, \quad (7)$$

where κ_u is the beamwidth of the user antenna. We consider that based on channel estimation, the reference BS and the typical user adjust their beam steering angles to achieve the maximum array gains. As a result of this, the total directivity gain of the desired signal is $G_b^{\max}G_u^{\max}$. Furthermore, for the lth interference link, the interfering user's boresight angle θ_u^l and the angle of arrival at the reference BS θ_b^l can be assumed as independently and uniformly distributed in $(0,2\pi]$, which results in a gain of $G_l=G_u(\theta_u^l)G_b(\theta_b^l)$. Hence, the directivity gain in the interference link G_l is a discrete random variable whose probability distribution is given in [12] as a_k with probability b_k $(k\in\{1,2,3,4\})$, where $a_1=G_b^{\max}G_u^{\max}, b_1=\frac{\kappa_b\kappa_u}{4\pi^2}, a_2=G_b^{\max}G_u^{\min}, b_2=\frac{\kappa_b}{2\pi}(1-\frac{\kappa_u}{2\pi}), a_3=G_b^{\min}G_u^{\max}, b_3=(1-\frac{\kappa_b}{2\pi})\frac{\kappa_u}{2\pi}, a_4=G_b^{\min}G_u^{\min}$ and $b_4=(1-\frac{\kappa_b}{2\pi})(1-\frac{\kappa_u}{2\pi})$.

D. User Fractional Power Control

We assume that each user utilizes a distance-proportional FPC of the form $R^{\alpha_0\tau}$, where $\tau\in[0,1]$ is the power control factor and α_0 is dependent on the FPC scheme assumption. Therefore, as a user moves closer to its associated BS, the transmit power required to achieve the target received signal power decreases. This is an important consideration in power limited devices such as the battery-powered mobile devices. In general, two FPC schemes can be identified for the mmWave cellular network:

1) Pathloss-based FPC: PL-FPC follows the same approach as in LTE and, hence, only the pathloss which is obtained via reference signals is required for its implementation [31]. PL-FPC operates by the compensating for the pathloss of a user irrespective of whether its path to its serving BS is LOS or NLOS. Hence, $\alpha_0=\alpha_L$ for a LOS user, and $\alpha_0=\alpha_N$ for a NLOS user.

[1]Note that the user association is not based on the instantaneous channel quality to avoid the ping-pong effect of handover that may occur due to the fast fluctuation of the instantaneous channel gain [18].

2) Distance-based FPC: D-FPC is based on the measured distance and always compensates by inverting with the LOS pathloss exponent, i.e., $\alpha_0 = \alpha_L$. As a result, in the D-FPC scheme, each user adjusts the transmit power as if the link to its serving BS were LOS, even if in fact it is NLOS. The scheme requires the knowledge of the user-BS distance which can be readily obtained, since the location of the BS is known while that of the user can be estimated by using GPS or position reference symbols. Note that with the PL-FPC scheme, the presence of a single NLOS user can result in significant performance degradation, as it will aim to compensate its NLOS path loss ($R^{-\alpha_N}$, where $\alpha_N \geq 4$) by transmitting at a high power, i.e., $R^{\alpha_N \tau}$ thereby causing significant interference to other users. Such effect is avoided with the D-FPC where the transmit power remains $R^{\alpha_L \tau}$, with typical α_L value of 2.

Moreover, if $\tau = 0$ in either scenario, no channel inversion is performed and all users transmit with the equal power.

E. Small-Scale Fading

We assume independent Nakagami fading for each link. In order to take the differences in the NLOS and LOS small-scale fading characteristic of mmWave propagation into consideration, we utilize different Nakagami fading parameters, N_L and N_N for the LOS and NLOS links, respectively. The parameters N_L and N_N are assumed to be positive integers for ease of tractability. Let g_l be the small-scale fading term on the lth link. Consequently, $|g_l|^2$ is a normalized Gamma random variable.

F. Dependence of the Distance of Interfering Users to their Serving BS

In order to model the uplink interference, we consider the typical user to be located at the origin and connected to the reference BS located at $\mathbf{B}_0$. We represent the set of interfering users by $\mathcal{Z}$, the distance of an interfering user $z \in \mathcal{Z}$ to the reference BS by $D_z = \|\mathbf{X}_z - \mathbf{B}_0\|$, and the distance of an interfering user to its serving BS by R_z. Based on this and the earlier assumptions, the SINR at the reference BS can be expressed as

$$\text{SINR} = \frac{|g_0|^2 G_b^{\max} G_u^{\max} L(R) R^{\alpha_0 \tau} P_b^0}{\sigma^2 + \sum_{z \in \mathcal{Z}} |g_z|^2 G_z L(D_z) R_z^{\alpha_0 \tau} P_b^0}, \tag{8}$$

where $|g_0|^2 G_b^{\max} G_u^{\max} L(R) R^{\alpha_0 \tau} P_b^0$ is the received power from the typical user at distance R from the reference BS, σ^2 is the noise power, G_z is the directivity gain on an interfering link and P_b^0 is a user or network specific parameter which is related to the target mean received power. Hence, characterizing the SINR coverage probability requires the knowledge of the distribution of R and R_z when a FPC scheme is implemented[2]. Moreover, the probability distribution function of a typical user at distance R from the reference has already been defined in (2) and (4) for LOS and NLOS associations, respectively. In order to characterize the distribution of R_z, it should be noted that the random variables $\{R_z\}_{z \in \mathcal{Z}}$ are identically distributed but not independent in general. This dependence is induced by the restriction of having one user served per-BS-per-channel, i.e., the coupling of the BS and served user-per channel point processes. However, as seen later in this section, this dependence is weak, which motivates the following independence assumption.

[2]Note that the distribution of R_z is not required for the case with fixed transmit power (no power control), i.e., $\tau = 0$.

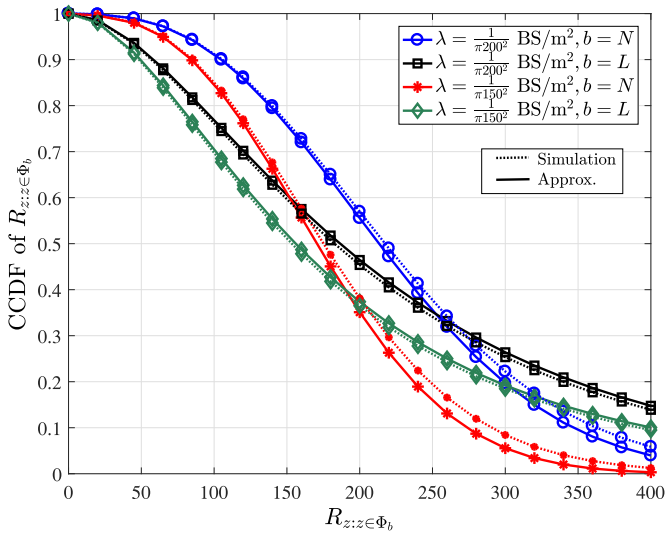

Fig. 2. A comparison of the CCDFs of $R_{z:z\in\Phi_b}$ for the PPP model with their simulation for $\lambda = \frac{1}{\pi 150^2}$ and $\frac{1}{\pi 200^2}$ BS/m^2.

Assumption 1 (Independence Assumption): We assume that the random variables $\{R_z\}_{z \in \mathcal{Z}}$ are independent and identically distributed (i.i.d). Since R_z can either be a LOS or NLOS association, the distributions of $R_{z:z\in\Phi_L}$ and $R_{z:z\in\Phi_N}$ can be approximated as $\mathcal{F}_{R_L}(r)$ and $\mathcal{F}_{R_N}(r)$, respectively, which are given in (2) and (4), respectively, which lends tractability to the analysis in the uplink of mmWave networks.

Validation of the Distribution of R_z: As mentioned in earlier, each BS serves a single user per channel at any time instant. Therefore, similar to the distance between the typical user and the reference BS, $R_{z:z\in\Phi_b}$ for $b \in \{L, N\}$ can be approximated as the distance of a randomly chosen point in $\mathbb{R}^2$, which can either be LOS or NLOS, to the BS that offers the maximum received power. Hence, its distribution can be approximated by

$$\begin{aligned} \mathcal{F}_{R_{zL}}(r_z) &= \mathcal{F}_{R_L}(r_z) \\ \mathcal{F}_{R_{zN}}(r_z) &= \mathcal{F}_{R_N}(r_z), \end{aligned} \tag{9}$$

where $\mathcal{F}_{R_L}(r_z)$ and $\mathcal{F}_{R_N}(r_z)$ are defined in (2) and (4), respectively, R_{zL} and R_{zN} are distance between LOS and NLOS interferers to their serving BS. The CCDF of $R_{z:z\in\Phi_b}$ for $b \in \{L, N\}$ is given by $\mathbb{P}[R_{z:z\in\Phi_b} > r_z] = \int_{r_z}^{\infty} \mathcal{F}_{R_{zb}}(x)\,\mathrm{d}x$, which is shown to be a close match for the Monte Carlo simulation of the approximated user PPP in Fig. 2 for $\lambda = \frac{1}{\pi 150^2}$ and $\frac{1}{\pi 200^2}$ BS/m^2. As far as the Monte Carlo simulation is concerned, we have followed the *Steps 1 to Step 5* described later in Section V. Although Fig. 2 shows that the approximation of the distribution of R_L, R_N and $R_{z:z\in\Phi_b}$, for $b \in \{L, N\}$, are accurate, it does not give any insight into the degree of dependence between the random variables $\{R_z\}_{z \in \mathcal{Z}}$ which is defined by their joint distribution. Since it is difficult to obtain insights from the

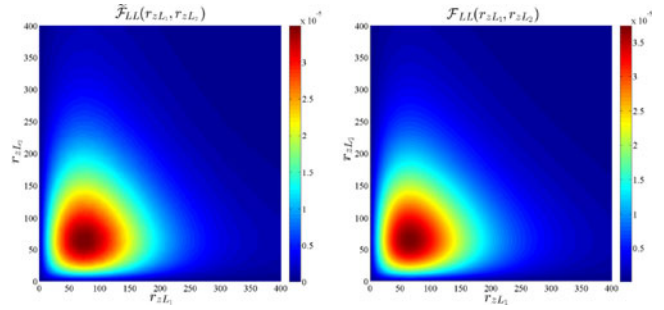

Fig. 3. Joint densities of R_{zL1} and R_{zL2} for the simulated PPP model (left) and the independence assumption (right). R_{zL1} and R_{zL2} are the distances of LOS users to their respective BSs in two neighboring cells.

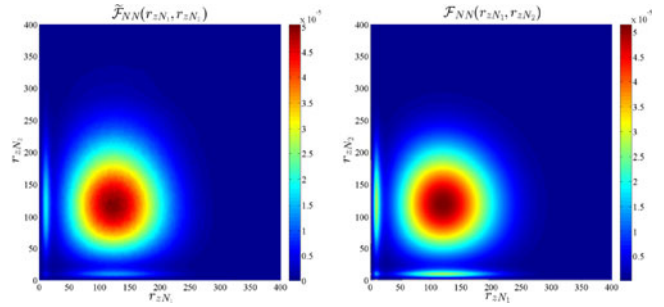

Fig. 4. Joint densities of R_{zN1} and R_{zN2} for the actual PPP model (left) and the independence assumption (right). R_{zN1} and R_{zN2} are the distances of NLOS users to their respective BSs in two neighboring cells.

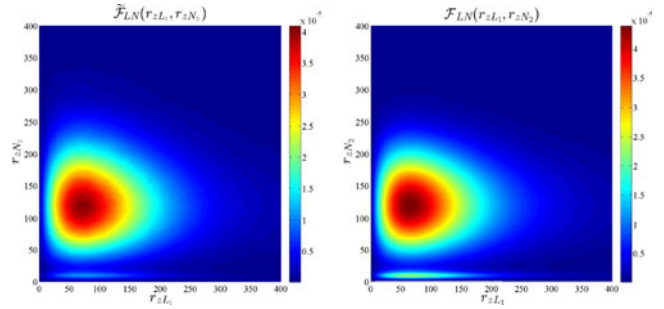

Fig. 5. Joint densities of R_{zL1} and R_{zN2} for the actual PPP model (left) and the independence assumption (right). R_{zL1} and R_{zN2} are the distances of LOS and NLOS users to their respective BSs in two neighboring cells.

complete joint distribution of $\{R_z\}_{z\in\mathcal{Z}}$, we focus on a much simplified scenario of the joint distribution of four random variables R_{zL1}, R_{zN1}, R_{zL2} and R_{zN2}, which are the distances of LOS and NLOS users to their respective BS in the two neighboring cells. Note that since the dependence is expected to be strongest in neighboring cells, this study illustrates the worst case scenario. Hence, we compute the joint pdfs $\widetilde{\mathcal{F}}_{R_{zL1},R_{zL2}}(r_{zL1},r_{zL2})$, $\widetilde{\mathcal{F}}_{R_{zN1},R_{zN2}}(r_{zN1},r_{zN2})$ and $\widetilde{\mathcal{F}}_{R_{zL1},R_{zN2}}(r_{zL1},r_{zN2})$ via Monte Carlo simulation and compare them with the joint pdfs under the independence assumptions in Figs. 3–5, respectively. The joint pdfs under the independence assumption follow directly from (2) and (4), and are given by:

$$\begin{aligned}\mathcal{F}_{R_{zL1},R_{zL2}}(r_{zL1},r_{zL2}) &= \mathcal{F}_{R_L}(r_{zL1})\mathcal{F}_{R_L}(r_{zL2})\\ \mathcal{F}_{R_{zN1},R_{zN2}}(r_{zN1},r_{zN2}) &= \mathcal{F}_{R_N}(r_{zN1})\mathcal{F}_{R_N}(r_{zN2})\\ \mathcal{F}_{R_{zL1},R_{zN2}}(r_{zL1},r_{zN2}) &= \mathcal{F}_{R_L}(r_{zL1})\mathcal{F}_{R_N}(r_{zN2}).\end{aligned} \tag{10}$$

From Figs. 3–5, we observe that the pdf obtained from the simulated PPP model and independence assumption are very similar. The correlation coefficient for $\rho_{R_{zL1},R_{zL2}}$, $\rho_{R_{zN1},R_{zN2}}$ and $\rho_{R_{zL1},R_{zN2}}$ are numerically computed as 0.00018, 0.0467 and -0.00137, respectively, in the simulation setup. Having validated the independence assumption, we now proceed to derive the SINR coverage probability.

III. SINR Coverage Probability

The SINR coverage probability $P_c(\Gamma)$ is defined as the probability that the received SINR at the reference BS is above a threshold Γ, i.e., $P_c(\Gamma)=\mathbb{P}(\text{SINR}>\Gamma)$. Theorem III.1 presents the SINR coverage probability with PL-FPC scheme. Moreover, since earlier simulation results in [7], [8] reveals that mmWave networks are more likely to be noise-limited in an urban setting, we also present the noise-limited approximation of the coverage probability. Hereafter, modifications required for the case with D-FPC scheme are presented as a corollary of Theorem III.1.

Theorem III.1: Using the generally tight approximation of the tail probability of a Gamma random variable in [32], the SINR coverage probability in the uplink of mmWave cellular networks with a PL-FPC scheme can be computed as

$$P_c(\Gamma)=\mathcal{A}_L P_{c,L}(\Gamma)+\mathcal{A}_N P_{c,N}(\Gamma), \tag{11}$$

where $P_{c,L}(\Gamma)$ and $P_{c,N}(\Gamma)$ are the conditional coverage probability given the reference BS serves a user in Φ_L and Φ_N, respectively, $\mathcal{A}_L$ and $\mathcal{A}_N$ are defined in (3) and (5), respectively. Moreover, $P_{c,b}(\Gamma)$, for $b\in\{L,N\}$, can be obtained as

$$\begin{aligned}P_{c,L}(\Gamma)\approx&\sum_{n=1}^{N_L}(-1)^{n+1}\binom{N_L}{n}\\&\times\int_0^\infty e^{-s_L\frac{\sigma^2}{P_b^0}-\sum_{o\in\{L,N\}}(G_o(\Gamma,r)+H_o(\Gamma,r))}\mathcal{F}_{R_L}(r)\mathrm{d}r\end{aligned} \tag{12}$$

$$\begin{aligned}P_{c,N}(\Gamma)\approx&\sum_{n=1}^{N_N}(-1)^{n+1}\binom{N_N}{n}\\&\times\int_0^\infty e^{-s_N\frac{\sigma^2}{P_b^0}-\sum_{o\in\{L,N\}}(J_o(\Gamma,r)+K_o(\Gamma,r))}\mathcal{F}_{R_N}(r)\mathrm{d}r\end{aligned} \tag{13}$$

where

$$\begin{aligned}G_o(\Gamma,r)=&-2\pi\lambda\mathcal{A}_o\\&\times\sum_{k=1}^{4}b_k\int_r^\infty F\left(N_L,s_L a_k y^{\alpha_o\tau}c^{-\alpha_L}\right)\mathrm{c}e^{-\beta c}dc\end{aligned} \tag{14}$$

$$H_o(\Gamma,r) = -2\pi\lambda\mathcal{A}_o \times \sum_{k=1}^{4} b_k \int_{\zeta_L(r)}^{\infty} F\left(N_N, s_L a_k y^{\alpha_o \tau} c^{-\alpha_N}\right)\left(1-e^{-\beta c}\right) c\mathrm{d}c \tag{15}$$

$$J_o(\Gamma,r) = -2\pi\lambda\mathcal{A}_o \times \sum_{k=1}^{4} b_k \int_{\zeta_N(r)}^{\infty} F\left(N_L, s_N a_k y^{\alpha_o \tau} c^{-\alpha_L}\right) e^{-\beta c} c\mathrm{d}c \tag{16}$$

$$K_o(\Gamma,r) = -2\pi\lambda\mathcal{A}_o \times \sum_{k=1}^{4} b_k \int_{r}^{\infty} F\left(N_N, s_N a_k y^{\alpha_o \tau} c^{-\alpha_N}\right)\left(1-e^{-\beta c}\right) c\mathrm{d}c, \tag{17}$$

$F(N,x) = 1 - \int_0^\infty \mathcal{F}_{R_o}(y)/(1+x)^N \mathrm{d}y$, $o \in \{L,N\}$, $s_L = \frac{\eta_L n r^{\alpha_L(1-\tau)}\Gamma}{G_u^{\max} G_b^{\max}}$, $s_N = \frac{\eta_N n r^{\alpha_N(1-\tau)}\Gamma}{G_u^{\max} G_b^{\max}}$, $\zeta_L(r) = (\frac{C_N}{C_L})^{\frac{1}{\alpha_N}} r^{\frac{\alpha_L}{\alpha_N}}$, $\zeta_N(r) = (\frac{C_L}{C_N})^{\frac{1}{\alpha_L}} r^{\frac{\alpha_N}{\alpha_L}}$, a_k and b_k are antenna directivity parameter defined in Section II-B. For $s \in \{L,N\}$ $\eta_s = N_s(N_s!)^{-\frac{1}{N_s}}$ and N_s are the parameter of the Nakagami small-scale fading.

Proof: See Appendix A.

For the noise-limited approximation, $\sigma^2 \gg \sum_{z\in\mathcal{Z}} g_z L(D_z) G_z R_z^{\alpha_0\tau}$, the signal-to-noise-ratio (SNR) coverage probability can be expressed from Theorem III.1 as

$$P_c(\Gamma) = \mathcal{A}_L \sum_{n=1}^{N_L} (-1)^{n+1} \binom{N_L}{n} \int_0^\infty e^{-\frac{\eta_L n \Gamma r^{\alpha_L(1-\tau)}}{G_u^{\max} G_b^{\max}} \frac{\sigma^2}{P_b^0}} \mathcal{F}_{R_L}(r)\mathrm{d}r + \mathcal{A}_N \sum_{n=1}^{N_N} (-1)^{n+1} \binom{N_N}{n} \int_0^\infty e^{-\frac{\eta_N n \Gamma r^{\alpha_N(1-\tau)}}{G_u^{\max} G_b^{\max}} \frac{\sigma^2}{P_b^0}} \mathcal{F}_{R_N}(r)\mathrm{d}r \tag{18}$$

by equating $G_o(\Gamma,r)$, $H_o(\Gamma,r)$, $J_o(\Gamma,r)$ and $K_o(\Gamma,r)$ to zero.

Corollary III.2: The SINR coverage probability in the uplink of mmWave cellular networks with D-FPC scheme can be computed as in (11) but with $\alpha_o = \alpha_L$ and $s_N = \frac{\eta_N n \Gamma r^{\alpha_N - \alpha_L \tau}}{G_u^{\max} G_b^{\max}}$ in (14)–(17).

A. SINR Coverage Probability With Fixed User Transmit Power

The SINR coverage probability can be simplified for the case with fixed user transmit power (i.e., $\tau = 0$), which is stated as the following corollary of Theorem III.1.

Corollary III.3: The SINR coverage probability in the uplink of mmWave cellular networks with fixed user transmit power can be expressed as in (11) but with $P_{c,b}(\Gamma)$, for $b \in \{L,N\}$, computed as

$$P_{c,L}(\Gamma) \approx \sum_{n=1}^{N_L} (-1)^{n+1} \binom{N_L}{n} \times \int_0^\infty e^{-s_L \frac{\sigma^2}{P_b^0} - G(\Gamma,r) - H(\Gamma,r)} \mathcal{F}_{R_L}(r)\mathrm{d}r \tag{19}$$

$$P_{c,N}(\Gamma) \approx \sum_{n=1}^{N_N} (-1)^{n+1} \binom{N_N}{n} \times \int_0^\infty e^{-s_N \frac{\sigma^2}{P_b^0} - J(\Gamma,r) - K(\Gamma,r)} \mathcal{F}_{R_N}(r)\mathrm{d}r, \tag{20}$$

where

$$G(\Gamma,r) = -2\pi\lambda \sum_{k=1}^{4} b_k \times \int_r^\infty e^{-\beta c} F\left(N_L, \frac{n\eta_L r^{\alpha_L}\Gamma a_k c^{-\alpha_L}}{G_u^{\max} G_b^{\max}}\right) c\mathrm{d}c \tag{21}$$

$$H(\Gamma,r) = -2\pi\lambda \sum_{k=1}^{4} b_k \times \int_{\zeta_L(r)}^\infty \left(1-e^{-\beta c}\right) F\left(N_N, \frac{n\eta_L r^{\alpha_L}\Gamma a_k c^{-\alpha_N}}{G_u^{\max} G_b^{\max}}\right) c\mathrm{d}c \tag{22}$$

$$J(\Gamma,r) = -2\pi\lambda \sum_{k=1}^{4} b_k \times \int_{\zeta_N(r)}^\infty e^{-\beta c} F\left(N_L, \frac{n\eta_N r^{\alpha_N}\Gamma a_k c^{-\alpha_L}}{G_u^{\max} G_b^{\max}}\right) c\mathrm{d}c \tag{23}$$

$$K(\Gamma,r) = -2\pi\lambda \sum_{k=1}^{4} b_k \times \int_r^\infty \left(1-e^{-\beta c}\right) F\left(N_N, \frac{n\eta_N r^{\alpha_N}\Gamma a_k c^{-\alpha_N}}{G_u^{\max} G_b^{\max}}\right) c\mathrm{d}c, \tag{24}$$

$F(N,x) = 1 - 1/(1+x)^N$, $\zeta_L(r) = (\frac{C_N}{C_L})^{\frac{1}{\alpha_N}} r^{\frac{\alpha_L}{\alpha_N}}$, $\zeta_N(r) = (\frac{C_L}{C_N})^{\frac{1}{\alpha_L}} r^{\frac{\alpha_N}{\alpha_L}}$, a_k and b_k are antenna directivity parameter defined in Section II-C. For $s \in \{L,N\}$ $\eta_s = N_s(N_s!)^{-\frac{1}{N_s}}$ and N_s are the parameter of the Nakagami small-scale fading

Proof: The proof follows directly from Theorem III.1 and the fact that $R_z^{\alpha_0\tau} = 1$ when $\tau = 0$.

B. SINR Coverage Probability With Simplified LOS Probability Function

The LOS probability function $p(x)$ can be simplified as a step function $S_{R_B}(x)$, where $S_{R_B}(x) = 1$ when $0 < x < R_B$, and $S_{R_B}(x) = 0$ otherwise. This implies that the LOS region observed by a typical user is characterized by a fixed disc of radius R_B. This simplification has been shown in [12] to provide a lower bound to the actual SINR distribution in the downlink of mmWave cellular networks with densely deployed BSs, where the dense classification implies that the LOS association probability $\mathcal{A}_L$ is greater than 0.95 and the parameter R_B has also been computed as $R_B = (\frac{-\ln(1-\mathcal{A}_L)}{\pi\lambda})^{0.5}$.

In order to obtain a more simplified expression for the SINR coverage probability, we further make the following assumptions

- Interference limited network: The performance of the network is interference limited in densely deployed BS scenario, hence the interference power $I \gg \sigma^2$ such that the thermal noise is ignored.
- No NLOS users: This is also as a result of the dense deployment of BSs which leads to all users having LOS paths to their serving BSs.

Following the above assumptions, which we validate in the numerical results section, we now present the SINR distribution in the uplink of a dense mmWave network. Our result is summarized in the following theorem.

Theorem III.4: The SINR coverage probability for the uplink of a dense mmWave network can be approximated as

$$P_c(\Gamma) = 2\pi\lambda \sum_{n=1}^{N} (-1)^{n+1} \binom{N}{n} \times \int_0^{R_B} r e^{-\pi\lambda r^2} \mathcal{L}_{I_r}\left(\frac{\eta n r^{\alpha_L(1-\tau)}\Gamma}{G_u^{\max} G_b^{\max}}\right) \mathrm{d}r, \quad (25)$$

where the Laplace transform of the interference is given by

$$\mathcal{L}(s) = e^{\left(-2\pi\lambda \sum_{k=1}^{4} b_k \int_r^{R_B} \left(1 - \int_0^{\infty} \frac{\pi\lambda e^{-\lambda\pi y}}{(1+s a_k c^{-\alpha_L} y^{\frac{\alpha_L \tau}{2}})^N} \mathrm{d}y\right) c \mathrm{d}c\right)}.$$

Proof: See Appendix B.

IV. Area Spectral Efficiency and Energy Efficiency Analysis

In this section, we utilize the developed framework in Section III to analyze the area spectral efficiency and energy efficiency in the uplink of mmWave cellular networks.

A. Rate and Area Spectral Efficiency

Here we turn our attention to the distribution of the achievable data rate Υ and the area spectral efficiency $\mathcal{S}$ in the uplink of mmWave cellular networks. The achievable data rate can be defined according to [12] as follows

$$\Upsilon = B \ln\left(1 + \min\left(\mathrm{SINR}, \Gamma_{\max}\right)\right), \quad (26)$$

where B is the bandwidth allocated to the user, $\Gamma_{\max}$ is the SINR threshold defined by the order of practical coding and modulation schemes, and the linearity of the radio frequency front-end.

The area spectral efficiency, which is the same as the potential throughput normalized by bandwidth can be obtained from the SINR coverage probability $P_c(\Gamma)$ by utilizing the following Lemma.

Lemma IV.1: Given the SINR coverage probability $P_c(\Gamma)$, the area spectral efficiency of the uplink of a mmWave cellular network can be expressed as

$$\mathcal{S} = \frac{\lambda}{\ln 2} \int_0^{\infty} \frac{P_c(\Gamma)}{1+\Gamma} \mathrm{d}\Gamma, \quad (27)$$

which has the unit of bps/Hz/m^2.

Proof: The proof follows directly from the relationship between the SINR coverage probability and the average ergodic spectral efficiency $\mathcal{R}$, which is given in [33], and the fact that $\mathcal{S} = \lambda\mathcal{R}$.

B. Energy Efficiency in the Uplink of mmWave Cellular Networks

In the previous sections, we have derived expressions for the SINR coverage probability and the area spectral efficiency of mmWave cellular networks based on PL-FPC and D-FPC. However, these metrics fail to give insights on how the energy consumed as a result of the two FPCs schemes compares. The recently introduced energy efficiency metric for communication systems gives such insights and is defined as the average amount of bits that can be delivered per joule consumed to do so [34]. Hence, the energy efficiency in the uplink of mmWave cellular networks is as follows

$$\mathcal{E}_{\mathrm{eff}} = \frac{\text{Area Spectral Efficiency}}{\text{Average Uplink Power Consumption}} = \frac{\mathcal{S}(\lambda)}{\lambda \mathcal{P}_{\mathrm{tot}}(\lambda)}, \quad (28)$$

where $\mathcal{S}(\lambda)$ is defined in (27) for both FPCs[3]. Note that $\mathcal{S}(\lambda)$ and $\mathcal{P}_{\mathrm{tot}}(\lambda)$ are both dependent on the type of FPC scheme that is implemented. In the following, we present the average uplink power consumption, $\mathcal{P}_{\mathrm{tot}}(\lambda)$, based on both the PL-FPC and D-FPC while assuming that all BSs are always kept on.

1) Average Uplink Power Consumption Based on PL-FPC: When the PL-FPC scheme is implemented, the average network power consumption $\mathcal{P}_{\mathrm{tot}}$ can be expressed as

$$\mathcal{P}_{\mathrm{tot}} = P_u + P_c + \Delta\left(\mathcal{A}_L \mathcal{P}_L(\lambda) + \mathcal{A}_N \mathcal{P}_N(\lambda)\right), \quad (29)$$

where P_c is the circuit power incurred by the user during transmission, P_u is the power consumed by the BS for processing uplink transmission, Δ quantifies the user device amplifier efficiency and $\mathcal{P}_b$ for $b \in \{L, N\}$ is the average transmit power of a typical user in Φ_b. $\mathcal{P}_b$ is obtained by averaging $\mathcal{P}_b(r)$ over distance r in Φ_b and is thus expressed as

$$\begin{aligned} \mathcal{P}_b(\lambda) &= \mathbb{E}\left[P_b^0 r^{\alpha_b \tau}\right] \\ &= \int_0^{\infty} P_b^0 r^{\alpha_b \tau} \mathcal{F}_{R_b}(r, \lambda) \mathrm{d}r \end{aligned} \quad (30)$$

where $\mathcal{F}_{R_b}(r, \lambda)$ for $b \in \{L, N\}$ is defined in (2) and (4), and P_b^0 as defined earlier in Section II is a user or network specific parameter which is related to target mean received power.

2) Average Uplink Power Consumption Based on D-FPC: The average network power consumption based on D-FPC scheme can be obtained as

$$\mathcal{P}_{\mathrm{tot}} = P_u + P_c + \Delta \bar{\mathcal{P}}_L(\lambda), \quad (31)$$

where

$$\begin{aligned} \bar{\mathcal{P}}_L(\lambda) &= \mathbb{E}\left[P_b^0 r^{\alpha_L \tau}\right] \\ &= 2\pi\lambda \int_0^{\infty} P_b^0 r^{(1+\alpha_L \tau)} \exp(-\lambda\pi r^2) \mathrm{d}r. \end{aligned}$$

[3] $P_c(\Gamma)$ is defined in Theorem III.1 and Corollary III.2 for the case with PL-FPC and D-FPC, respectively.

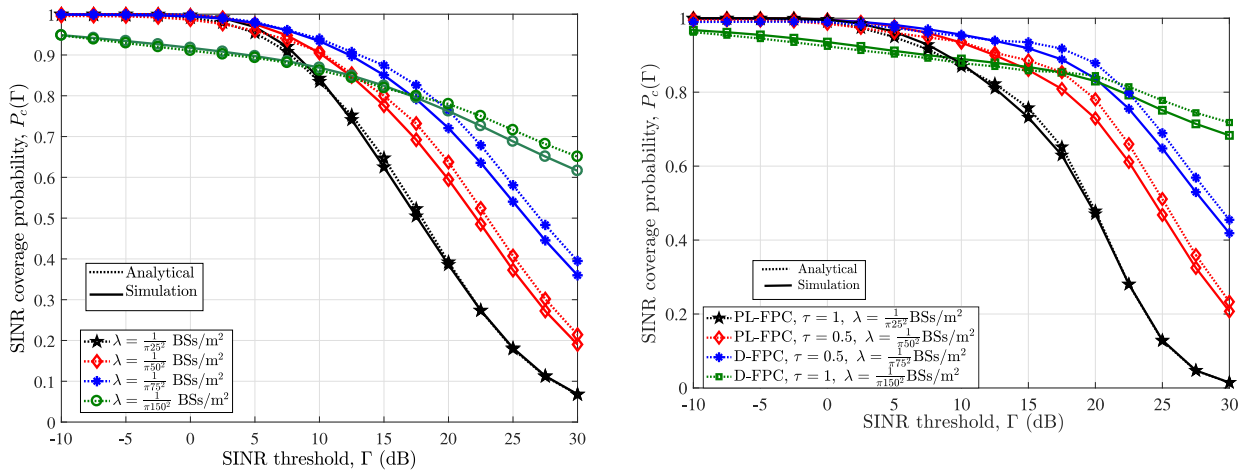

Fig. 6. SINR coverage probability in the uplink channel of mmWave cellular networks. (a) No power control ($\tau = 0$). (b) Fractional power control ($\tau = 0.5, 1$).

Note that in an ideal scenario, the average power consumption for both FPC schemes is equivalent to the average transmit power of the typical user, i.e., $\bar{\mathcal{P}}_L(\lambda)$ and $\mathcal{A}_L\mathcal{P}_L(\lambda) + \mathcal{A}_N\mathcal{P}_N(\lambda)$, for the D-FPC and PL-FPC schemes, respectively. Since $P_u \to 0, P_c \to 0$ and $\Delta \to 1$ in (29) and (31) in the ideal case.

C. Fairness Analysis of the Fractional Power Control Schemes

As mentioned earlier in Section II-D, in the D-FPC scheme, each user adjusts the transmit power as if the link to its serving BS were LOS, even if in fact it is NLOS. As a result, the D-FPC scheme is often favorable compared to PL-FPC scheme in terms of interference, since D-FPC prevents the NLOS users from transmitting with too much power and producing too much interference. However, one disadvantage of D-FPC is that it tends to be unfair to the NLOS users, who are being forced to use a lower transmit power than under PL-FPC. Hence, we investigate the fairness of the two FPC schemes using the Jain's fairness equation [35] which is expressed as

$$\mathcal{J}(R_1, R_2, \ldots, R_n) = \frac{\left(\sum_{i=1}^{n} R_i\right)^2}{n\sum_{i=1}^{n} R_i^2}, \tag{32}$$

where there are n users and R_i is the average spectral efficiency of the i^{th} link. Noting that a typical user can be LOS and NLOS with the reference BS with probability $\mathcal{A}_L$ and $\mathcal{A}_N$, respectively and that the average ergodic spectral efficiency of LOS and NLOS users are $\mathcal{R}_L$ and $\mathcal{R}_N$, respectively, the Jain fairness can be evaluated as

$$\widetilde{\mathcal{J}}(\mathcal{R}_L, \mathcal{R}_N) = \frac{\left(\mathcal{A}_L\mathcal{R}_L + \mathcal{A}_N\mathcal{R}_N\right)^2}{\mathcal{A}_L\mathcal{R}_L^2 + \mathcal{A}_N\mathcal{R}_N^2}. \tag{33}$$

V. Numerical Results

In this section, we present numerical results to demonstrate the accuracy of the analytical expressions derived in Section III and IV. We assume that the mmWave network is operated at 28 GHz with 100 MHz allocated to each user. The LOS and NLOS pathloss exponents are taken as $\alpha_L = 2$ and $\alpha_N = 4$, respectively. Furthermore, we assume that the LOS probability function $p(R) = e^{-\beta R}$, where $1/\beta = 141.4$ m. The Nakagami fading parameters are $N_L = 3$ and $N_N = 2$. The antenna gain pattern of a BS is assumed to be characterized with $G_b^{\max} = 10$ dB, $G_b^{\min} = -10$ dB and $\kappa_b = 30°$, while that of a user is assumed to be characterized with $G_u^{\max} = 10$ dB, $G_u^{\min} = -10$ dB and $\kappa_u = 90°$. For comparison purposes, we also consider the conventional UHF cellular network operated at 2 GHz. The stochastic geometry analytical framework in [17], which does not differentiate between LOS and NLOS transmission, and also considers a small-scale Rayleigh fading between users and BSs is utilized for the performance evaluation of conventional UHF architecture. Only one pathloss exponent is defined in [17], which is denoted as α and set here as $\alpha = \alpha_N$. Furthermore, for fairer comparison we also consider the SINR coverage probability of the UHF network with Nakagami fading parameter $N = 2$.

1) Accuracy of Analytical Framework: In Fig. 6, we compare the SINR coverage probability obtained via our analytical framework in Theorem III.1 with the Monte Carlo simulations for FPC factors $\tau = 0, 0.5, 1$, and BS densities $\lambda = \frac{1}{\pi 25^2}, \frac{1}{\pi 50^2}, \frac{1}{\pi 75^2}$ and $\lambda = \frac{1}{\pi 150^2}$ BSs/m^2. As far as Monte Carlo Simulation of the SINR coverage probability is concerned, we have used the following method

1) For a fixed average number of BSs, $\overline{N} = 200$, a fixed circular area of radius $R_A = \sqrt{\frac{\overline{N}}{\pi\lambda}}$ is considered. The number of BSs (equivalently the radius R_A) is chosen sufficiently large to have a small error between the analytical results obtained on the infinite plane and the numerical results obtained from a finite disc.
2) $N_u \gg \overline{N}$ users are uniformly distributed over the circular region of area $\pi {R_A}^2$.
3) The number of BS $\widetilde{N}$ is generated following a Poisson distribution with density λ and area $\pi {R_A}^2$, and uniformly distributed over the circular region of area $\pi {R_A}^2$.
4) The user-BS association as described in Section II-A is applied such that each user is associated with the BS that offers the maximum received signal.

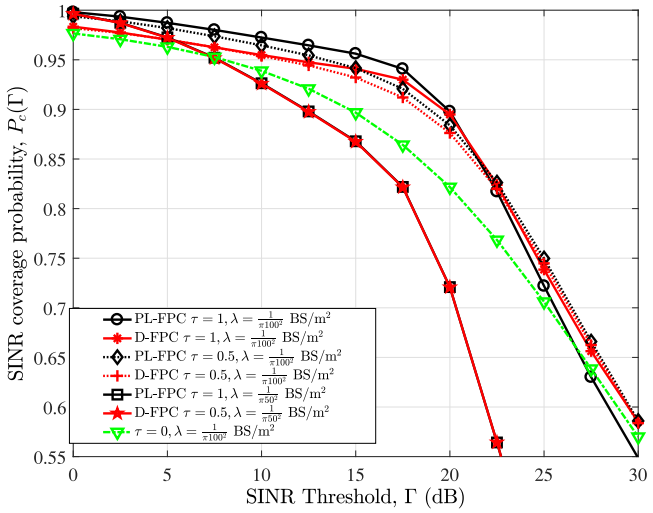

Fig. 7. Comparison of the SINR coverage probability based on the PL-FPC and the D-FPC in the uplink of mmWave cellular networks.

5) Each BS utilizes a round-robin scheduler, and randomly selects the served user. The origin is shifted to the location of the probe typical user whose connected BS is termed the reference BS.
6) For the simulation trial i, due to the random channel gains, we compute the SINR coverage probability by running an embedded simulation.
   a) Generate the Nakagami fading channel gain for each link with LOS and NLOS links having the Nakagmi fading parameters $N_L = 3$ and $N_N = 2$, respectively.
   b) The SINR is computed as shown in (6). If the computed SINR $\geq \Gamma$, increment the counter κ by 1.
   c) The SINR coverage probability for the i^{th} simulation trial ϵ_i is computed by repeating the *Step a* and *Step b* for N_v times, and eventually $\epsilon_i = \frac{\kappa}{N_v}$.
7) Finally, the average SINR coverage probability over all simulation trials is computed by repeating the *Step 1–Step 6* for N_{mc} times, and eventually calculating $P_c(\Gamma) = \frac{1}{N_{mc}} \sum_{i=1}^{N_{mc}} \epsilon_i$. In our simulations, we have considered $N_u = \overline{N}^2$, $N_v = 10^2$ and $N_{mc} = 10^5$.

The results in Fig. 6 show that the analytical results obtained from Theorem III.1 closely match with the simulation results. Note that the analytical results are based on 1) the independence assumption and 2) the uniform distribution of the angles of arrival with respect to the boresight angle. The results in Fig. 6 further validates the accuracy of the independence assumption presented earlier in Figs. 3–5. Though the gap between derived expressions and simulation results stays small for all tested scenarios, this gap becomes negligible as the density of BS grows. As future mmWave networks are expected to have high BS density, the derived expressions provide a highly accurate method to estimate the uplink coverage probability for future mmWave networks.

2) D-FPC vs PL-FPC: Fig. 7 compares the performance of the D-FPC and PL-FPC schemes for FPC factors $\tau = 0.5$ and 1, and BS densities $\frac{1}{\pi 50^2}$ and $\frac{1}{\pi 100^2}$ BS/m^2. Both power control schemes are also benchmarked with the case without power control, i.e., $\tau = 0$. The results in Fig. 7 show that the D-FPC scheme has greater coverage at high SINR thresholds, for $\lambda = \frac{1}{\pi 100^2}$ BS/m^2 and full FPC, i.e., $\tau = 1$, compared with the PL-FPC scheme. This is due to the fact that more users suffer from higher interference as a result of the NLOS users' channel inversion in the PL-FPC scheme, hence, a higher proportion of users are with lower SINR in PL-FPC. The coverage margin between the two FPC methods, however, reduces as the FPC factor is reduced to 0.5. Furthermore, as the BS density is increased, to $\frac{1}{\pi 50^2}$ BS/m^2, the D-FPC and PL-FPC converge. This is due to the fact that increasing the BS density increases the tendency of having LOS association and hence, PL-FPC converges to D-FPC when $\mathcal{A}_L \to 1$.

3) Effect of FPC Factor τ: As mentioned earlier in Section II-D, the main motivation for implementing FPC in the uplink of a cellular network is to provide coverage improvement for the lowest-percentile users and minimize the power consumption (transmit power) of battery-powered users. Hence, it is of utmost importance to select the optimal FPC factor for each user in order to achieve acceptable performance for most users and improved system capacity [31]. Fig. 8 gives the SINR coverage probability distribution as a function of the FPC factor τ for the PL-FPC and D-FPC schemes and $\lambda = \frac{1}{\pi 100^2}$ BSs/m^2. The baseline approach that applies a fixed transmit power for all users ($\tau = 0$) yields the lowest overall coverage in both D-FPC and PL-FPC plots in Fig. 8(a) and (b), respectively. The largest SINR coverage probability for users in the lower 90 percentile is achieved by $\tau > 0.5$ in both FPC schemes. In addition, FPC factor, $\tau = 0.5$, gives the best SINR coverage probability when $\Gamma \gtrsim 25$ dB. Hence, for both FPC schemes, either $\tau = 0.5, 0.75$ or $\tau = 1$ can achieve the maximum coverage. This is contrary to what was observed for the conventional UHF network in [17], where FPC factor $\tau < 0.5$ achieved the highest SINR coverage probability. The discrepancy is due to the likelihood that an interfering user will be blocked in the mmWave network. Hence, the high FPC factor of the interfering users will have less impact as compared with the conventional UHF network which does not experience such blockage effect. Fig. 8 also plots the SINR coverage probability for the case without directional beamforming. As it can be seen, implementing directional beamforming results in significant improvement in the coverage since narrow beams lead to an increase in the SNR and reduction in the interference leakage. Hence, FPC should be implemented with beamforming.

4) Effect of BS Density: In Fig. 9, we plot the coverage probability distribution as a function of the BS density for the mmWave and UHF networks, and for the case with no power control $\tau = 0$ and full power control (PL-FPC and D-FPC) $\tau = 1$. For the case without power control ($\tau = 0$) in Fig. 9(a), the coverage probability performance obtained from the stochastic geometry analysis for the UHF network, initially increases with the BS density. This is due to the fact that having more BSs lead to improved coverage in the noise-limited network (i.e. eliminates coverage hole). When λ is large enough (e.g., $\lambda > 10^{-1}$ BSs/km^2), the SINR coverage probability becomes independent of the BS density as the network becomes interfer-

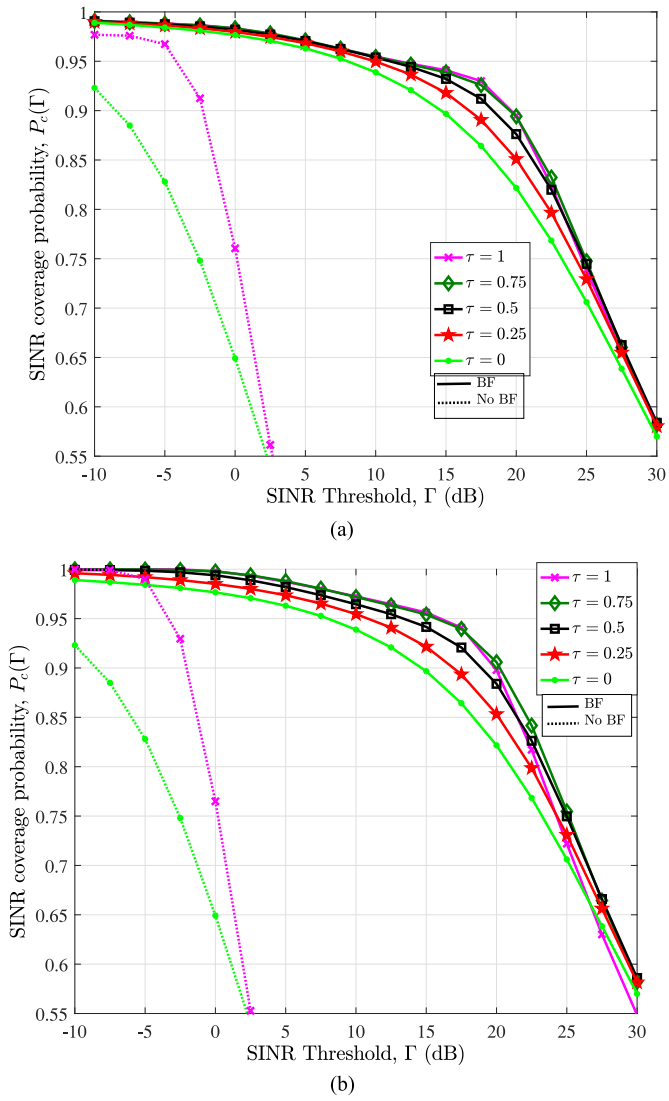

Fig. 8. Uplink SINR coverage probability with distance based FPC and pathloss based FPC, and a range of τ values. (a) D-FPC approach. (b) PL-FPC approach.

ence limited. This observation is consistent with the downlink conclusions in [16], [26], which shows that for a sufficiently large BS density, the coverage probability becomes almost a constant with the increase of the BS density. The simple pathloss model is responsible for this behavior as the increased interference is being counterbalanced by the received signal power as λ increases in the interference limited network. In the mmWave network, the same observation, which follows the UHF reasoning, is experienced in the noise-limited region. However, when the mmWave network becomes denser than a certain threshold, the coverage probability starts decreasing. The reason behind this is that NLOS interference paths are converted to LOS path interference paths. To gain more insight, we plot Fig. 10 which compares the performance of the mmWave network with LOS and NLOS paths with the mmWave network with 1) only LOS paths 2) only NLOS paths, for the case with no power control. As it can be seen, the SINR coverage probability of the mmWave network with LOS and NLOS paths converges to that with only NLOS in at low BS density, and to that with only LOS at high BS density.

For the case with full power control in Fig. 9(b), increasing the BS density does not have any impact on the SINR coverage probability of the UHF network. On the contrary, the coverage probability of the mmWave framework with PL-FPC scheme remains the same with increasing BS density until a threshold where it starts rising to its peak and then decreases afterward. Implementing full power control for the UHF network implies that the transmit power of all users reduces as the BS density increases and hence, the SINR coverage probability remains unaffected. Whereas in the mmWave network, NLOS paths convert to LOS paths as the BS density increases. This results in the reduction of the users transmit power, which causes an initial increase in the SINR coverage probability. However, similar to mmWave network with no power control, the likelihood of having an LOS interferer also increases. This consequently results in the reduction in the SINR coverage probability as its effect eventually predominated that of the transmit power reduction. Regarding the D-FPC scheme, it outperforms the PL-FPC scheme at low BS density and converges to the PL-FPC at high BS density. This convergence is expected since all paths become LOS at very high BS density. Furthermore, for the UHF network with Nakagami fading, it can be observed that its SINR coverage probability converges to that of mmWave without power control when $\lambda < 10^{-0.2}$ BS/km^2. A similar observation can be seen for the PL-FPC scheme with full power control.

It can be further observed from Fig. 9(a) and (b) that the FPC factor that maximizes the SINR coverage probability in the mmWave network is also a function of the BS density. For a given SINR threshold, Γ, and for a given FPC factor τ, there exists a BS density that maximizes the SINR coverage probability. Take for example, $\Gamma = 30$ dB and $\tau = 0$ in Fig. 9(a), the SINR coverage probability is maximized at a BS density of 10 BSs/km^2 while achieving a coverage of 65%, whereas the coverage probability is maximized at a BS density of 40 BSs/km^2 while achieving 60% coverage for $\Gamma = 30$ dB and PL-FPC with $\tau = 1$ in Fig. 9(b).

In Fig. 11, we show the results based on the SNR coverage probability, which has been obtained from the noise-limited approximation of the SINR coverage probability in (18), and for $\tau = 0$. It can be observed that the SNR coverage probability tracks the SINR coverage probability for a threshold $\Gamma < 5$ dB and BS density $\lambda < 10^{-1.8}$ BSs/km^2. However, for very large BS densities, the interference dominates and a gap can be seen between the SINR and SNR coverage plots.

5) Accuracy of Framework With Simplified LOS Function: In Fig. 12, we show the results based on the dense network analysis of Section III-B. It can be observed that the accuracy of the simplified model given in (25), which is based on interference limited network and no NLOS-user assumptions, increases as the BS density increases. Hence the assumptions and simplifications made in Section III-B are valid in very dense BS deployments.

6) Area Spectral Efficiency: Fig. 13 gives the area spectral efficiency of both mmWave and UHF networks as a function of BS density λ, for FPC $\tau = 0$ and 1. As it can be observed, the

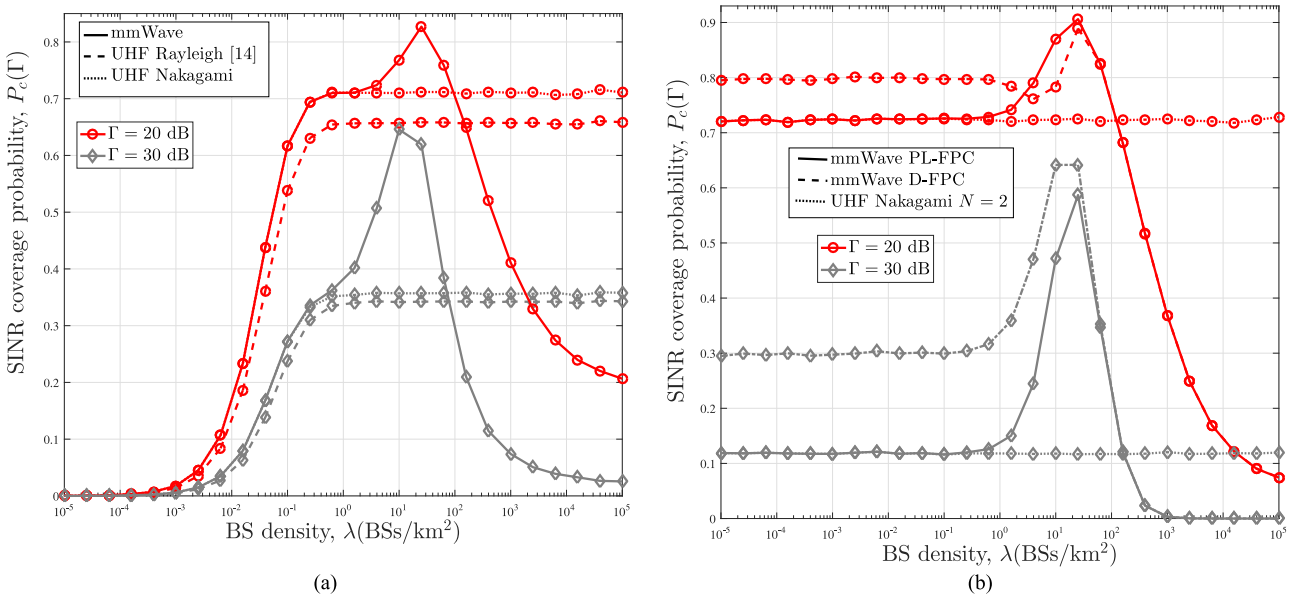

Fig. 9. Comparison of the SINR coverage probability of the mmWave and UHF networks in the uplink channel. (a) The power control factor $\tau = 0$. (b) The power control factor $\tau = 1$.

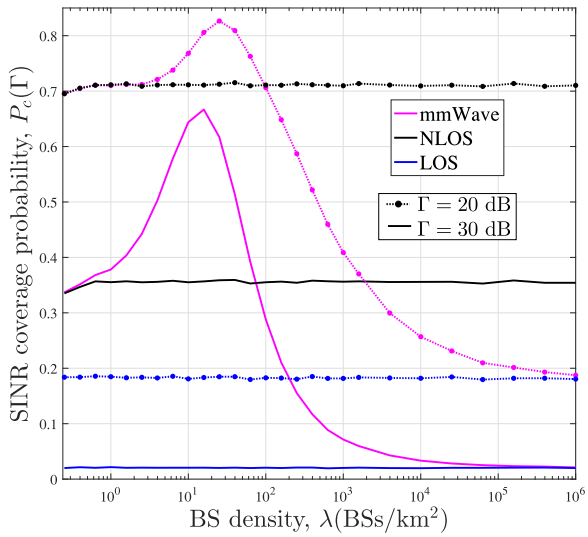

Fig. 10. SINR coverage probability in the uplink of mmWave networks.

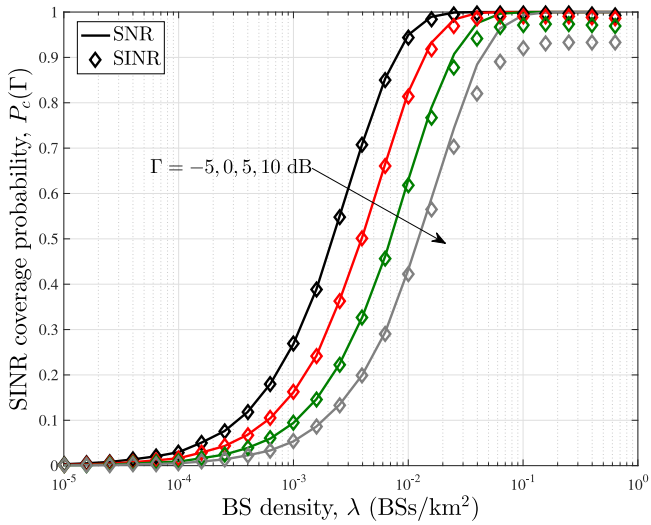

Fig. 11. Comparison of SINR and SNR coverage probability in the uplink of mmWave cellular networks.

area spectral efficiency of the UHF network with $\tau = 0$ increases invariably-linearly with λ, when λ is large enough, e.g. $\lambda \geq 10^{-1}$ BS/km^2. Whereas, for $\tau = 1$, its area spectral efficiency increases linearly without a restriction on λ. This can be implied from the result in Fig. 9 where the SINR coverage probability of the UHF model becomes constant with increased λ, i.e., $\lambda \geq 10^{-1}$ BS/km^2 for $\tau = 0$, while the SINR coverage probability is constant over all λ values for $\tau = 1$. On the other hand, the mmWave network experiences a slow growth region between $\lambda = 10^1$ BS/km^2 and $\lambda = 10^3$ BS/km^2, which is due to the sharp decrease in the SINR coverage probability at that region. The results also show that the area spectral efficiency of the mmWave network with D-FPC converges to that with PL-FPC as the BSs become very dense ($\lambda \geq 10^2$ BS/km^2). Furthermore, the area spectral efficiency of the mmWave network (with PL-FPC) converges to that of the UHF model when $\lambda \leq 10^{-0.2}$ BS/km^2 and $\lambda \leq 10^{-1.4}$ BS/km^2, for $\tau = 1$ and $\tau = 0$, respectively. A similar trend in SINR coverage probability and area spectral efficiency performances have been observed for the downlink channel of mmWave networks in [26].

7) Energy Efficiency and Rate Fairness: Fig. 14 shows the energy efficiency and fairness of the two FPC schemes for $\tau = 0.75$ and 1, $P_u = 1.2$ W, $P_b^0 = -29$ dBm, $P_c = 0.1$ W and $\Delta = 1$. To gain insight into the energy efficiency performance of the two schemes, the average transmit power with these configurations are illustrated in the lower-right graphs of Fig. 14. The results in the lower-right graphs indicate that

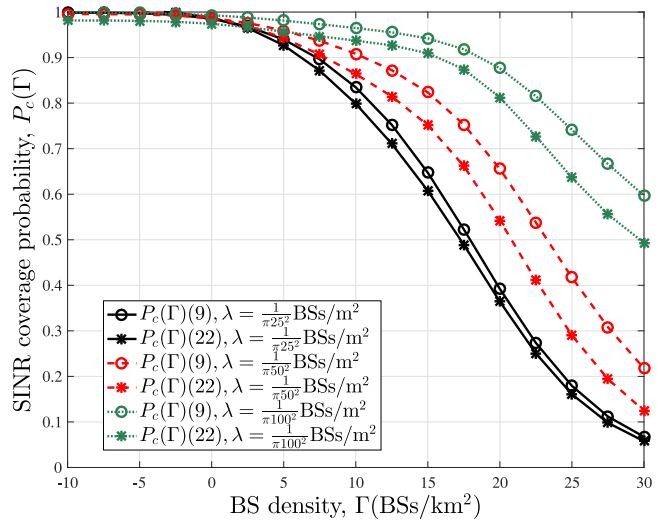

Fig. 12. SINR coverage probability with $p(r)$ being approximated by a step function $S_{R_B}(t)$ in the uplink of mmWave cellular networks.

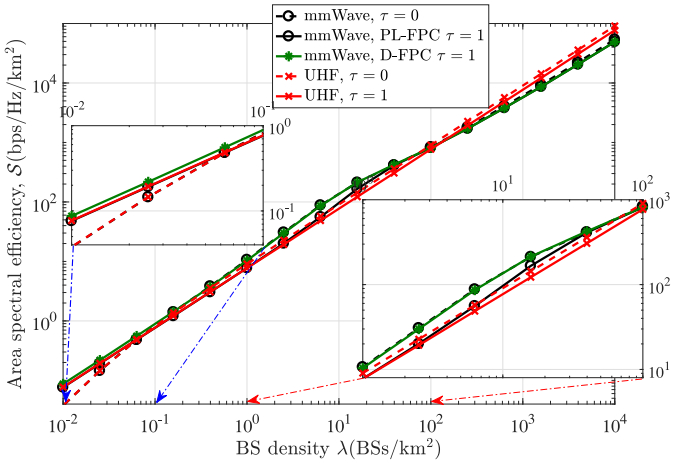

Fig. 13. Comparison of the area spectral efficiency of the mmWave and UHF networks in the uplink channel for $\tau = 0$ and $\tau = 1$.

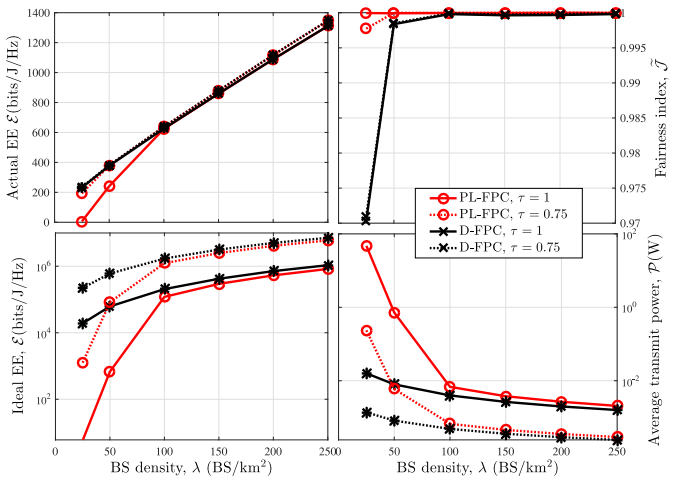

Fig. 14. Comparison of the energy efficiency performance of the D-FPC and PL-FPC in the uplink mmWave cellular networks. We assume that all users transmit using a FPC factor $\tau = 0.75$ and 1.

implementing a PL-FPC scheme leads to a higher average transmit power compared with the D-FPC scheme. In the lower-left graph, we plot the ideal energy efficiency which can be obtained from (28), but with $P_u = 0, P_c = 0$ and $\Delta = 1$. As it can be observed, implementing D-FPC scheme leads to an improvement in the ideal energy efficiency performance. The improved performance is as a result of the higher area spectral efficiency and the lower average transmit power experienced with the D-FPC scheme. The actual energy efficiency, which is based on the realistic power consumption model is illustrated in the upper-left graph. It can be observed that the D-FPC scheme still outperforms the PL-FPC scheme but with a much lower margin. Furthermore, operating at a FPC factor $\tau = 0.75$ yields a higher energy efficiency (ideal and actual) in both FPCs. In the upper-right graph, we plot the fairness of the two FPC schemes. The result shows that the PL-FPC scheme exhibits a higher fairness index compared with the D-FPC. This is due to the fact that in full FPC with $\tau = 1$, PL-FPC scheme achieves equal received signal strength for all user by compensating the pathloss for both NLOS and LOS users, and hence, all users experience the same performance. Whereas, full pathloss compensation is only achieved for the LOS users in the D-FPC scheme thus leading to a reduction in its fairness. Nevertheless, the fairness index of D-FPC approaches that of PL-FPC as the BS density increases.

VI. Conclusion

In this paper, we have presented a stochastic geometry framework to analyze the SINR coverage in the uplink of millimeter wave (mmWave) cellular networks. The framework takes the effect of blockage into consideration by utilizing a distance-dependent line-of-sight (LOS) probability function and modeling the location of LOS and non-LOS users as two independent non-homogeneous Poisson point processes. The proposed model takes into account the per-user fractional power control (FPC), which couples the transmission of users due to location-dependent channel inversion. Two FPC schemes are modeled into the framework: 1) distance-based FPC (D-FPC) which is based on the measured distance and 2) pathloss-based FPC (PL-FPC) which is the conventional approach and is based on the measured pathloss. Based on the proposed framework, we have derived the expression for the SINR coverage probability in the uplink of mmWave cellular networks, which was shown to be a good fit with the simulation. Numerical results show that the D-FPC outperforms the PL-FPC approach in terms of SINR coverage at the high SINR threshold. Next, we simplified the expression for the case with fixed transmit power and when the LOS region is modeled as a fixed-size equivalent LOS disc. Results showed that the simplified LOS region gives a good fit in very dense networks. Hereafter, we derived the area spectral efficiency, energy efficiency, and fairness expressions. In terms of the area spectral efficiency and energy efficiency, the D-FPC scheme gives better or equivalent performance compared with the PL-FPC scheme. On the other hand, the PL-FPC scheme achieves a higher fairness index compared with the D-FPC scheme. Lastly, contrary to the ultra-high frequency cellular networks, the SINR coverage in mmWave cellular networks de-

creases as the cell density becomes greater than a threshold while its area spectral efficiency experiences a slow growth region.

Note that the coverage probability presented in this paper was based on the sectored antenna model for analytical tractability. As recently shown in [36], the sectored model presents a lower bound to the coverage probability when the actual antenna pattern is utilized. Hence, the coverage probability which captures more accurate antenna pattern deserves attention in a future study.

APPENDIX

A. Proof of Theorem III.1

Given that the link between the desired (typical) user and the reference BS is LOS, the conditional coverage probability can be computed as

$$P_{c,L}(\Gamma) = \int_0^\infty \mathbb{P}[\text{SINR} > \Gamma]\mathcal{F}_{R_L}(r)\mathrm{d}r$$
$$= \int_0^\infty \mathbb{P}\left[|g_0|^2 > r^{\alpha_L(1-\tau)}\Gamma Q/(G_u^{\max}G_b^{\max})\right]\mathcal{F}_{R_L}(r)\mathrm{d}r \tag{34}$$

where

$$Q = I_{LL} + I_{LN} + I_{NL} + I_{NN+}\sigma^2/P_b^0,$$
$$I_{LL} = \sum_{l:X_l\in\Phi_L\cap\bar{\mathcal{B}}(0,r)\cap L} |g_l|^2 G_l D_l^{-\alpha_L} R_l^{\alpha_L\tau},$$
$$I_{LN} = \sum_{l:X_l\in\Phi_L\cap\bar{\mathcal{B}}(0,r)\cap N} |g_l|^2 G_l D_l^{-\alpha_L} R_l^{\alpha_N\tau},$$
$$I_{NL} = \sum_{l:X_l\in\Phi_N\cap\bar{\mathcal{B}}(0,\zeta_L(r))\cap L} |g_l|^2 G_l D_l^{-\alpha_N} R_l^{\alpha_L\tau},$$

and $I_{NN} = \sum_{l:X_l\in\Phi_N\cap\bar{\mathcal{B}}(0,\zeta_L(r))\cap N} |g_l|^2 G_l D_l^{-\alpha_N} R_l^{\alpha_N\tau}$ are the interferences experienced at the reference BS from the LOS users with LOS links to their serving BSs, LOS users with NLOS links to their serving BSs, NLOS users with LOS links to their serving BSs and NLOS users with NLOS links to their serving BSs, respectively, $\mathcal{B}(0,r)$ denotes a disc of radius r and $\bar{\mathcal{B}}(0,r)$ denotes outside $\mathcal{B}(0,r)$. L and N are sets of interfering users with LOS link and NLOS link, respectively, to their serving BS. The CCDF of the SINR at distance r from the reference BS is

$$\mathbb{P}\left[|g_0|^2 > r^{\alpha_L(1-\tau)}\Gamma Q/(G_u^{\max}G_b^{\max})\right]$$
$$\overset{(a1)}{\approx} 1 - \mathbb{E}_\Phi\left[\left(1-\exp\left(\frac{-\eta_L r^{\alpha_L(1-\tau)}\Gamma Q}{G_u^{\max}G_b^{\max}}\right)\right)^{N_L}\right]$$
$$\overset{(a2)}{=} \sum_{n=1}^{N_L}(-1)^{n+1}\binom{N_L}{n}\mathbb{E}_\Phi\left[\exp\left(\frac{-\eta_L n r^{\alpha_L(1-\tau)}\Gamma Q}{G_u^{\max}G_b^{\max}}\right)\right]$$
$$\overset{(a3)}{=} \sum_{n=1}^{N_L}(-1)^{n+1}\binom{N_L}{n}\exp\left(-s_L\frac{\sigma^2}{P_b^0}\right)\prod_{i,j\in L,N}\mathcal{L}_{I_{i,j}}(s_L) \tag{35}$$

where $s_L = \frac{\eta_L n r^{\alpha_L(1-\tau)}\Gamma}{G_u^{\max}G_b^{\max}}$, $\eta_L = N_L(N_L!)^{-\frac{1}{N_L}}$, $(a1)$ follow from the fact that $|g_0|^2$ is a normalized gamma random variable with parameter N_L and the fact that for a constant $\gamma > 0$, the probability $\mathbb{P}(|g_0|^2 < \gamma)$ is tightly upper bounded by $[1-\exp(-\gamma N(N!)^{-\frac{1}{N}})]^N$ [32]. $(a2)$ follows from the binomial theorem and the earlier assumption that N_L is a positive integer, and $(a3)$ follows from the definition of Laplace transform of interference $\mathcal{L}_{I_{i,j}}(s_L) = \mathbb{E}_{I_{i,j}}[e^{-s_L I_{i,j}}]$. To complete the derivation, stochastic geometry concepts can be applied to derive the expression for $\mathcal{L}_{I_{LL}}(s_L)$ in (35) as

$$\mathcal{L}_{I_{LL}}(s_L)$$
$$= \mathbb{E}_{I_{LL}}[e^{-s_L I_{LL}}]$$
$$= \mathbb{E}_{\Phi_L}\left[\exp\left\{-s_L\sum_{z:X_z\in\Phi_L\cap\bar{\mathcal{B}}(0,r)\cap L}|g_z|^2 G_z D_z^{-\alpha_L} R_z^{\alpha_L\tau}\right\}\right]$$
$$= \mathbb{E}_{R_z,G_z,D_z,g_z}$$
$$\times\left[\prod_{z:X_z\in\Phi_L\cap\bar{\mathcal{B}}(0,r)\cap L}\exp\left\{-s_L|g_z|^2 G_z D_z^{-\alpha_L} R_z^{\alpha_L\tau}\right\}\right]$$
$$= \mathbb{E}_{G_z,D_z}$$
$$\times\left[\prod_{z:X_z\in\Phi_L\cap\bar{\mathcal{B}}(0,r)\cap L}\mathbb{E}_{R_z,g_z}\left[\exp\left\{-s_L|g_z|^2 G_z D_z^{-\alpha_L} R_z^{\alpha_L\tau}\right\}\right]\right]$$
$$\overset{(a4)}{=} e^{\left(-2\pi\lambda\mathcal{A}_L\sum_{k=1}^4 b_k\int_r^\infty e^{-\beta c}\left(1-\mathbb{E}_{R_z,g}\left[e^{-s_L a_k g c^{-\alpha_L} R_z^{\alpha_L\tau}}\right]\right)c\mathrm{d}c\right)}$$
$$\overset{(a5)}{=} e^{\left(-2\pi\lambda\mathcal{A}_L\sum_{k=1}^4 b_k\int_r^\infty e^{-\beta c}\left(1-\mathbb{E}_{R_z}\left[\frac{1}{1+s_L a_k c^{-\alpha_L} R_z^{\alpha_L\tau}}\right]^{N_L}\right)c\mathrm{d}c\right)}$$
$$\overset{(a6)}{=} \prod_{k=1}^4 e^{\left(-2\pi\lambda\mathcal{A}_L b_k\int_r^\infty e^{-\beta c}\left(1-\int_0^\infty\frac{\mathcal{F}_{R_L}(y)}{(1+s_L a_k c^{-\alpha_L} y^{\alpha_L\tau})^{N_L}}\mathrm{d}y\right)c\mathrm{d}c\right)}$$
$$= e^{-G_L(\Gamma,r)}, \tag{36}$$

where g in $(a4)$ is a normalized gamma variable with parameter N_L a_k and b_k are defined in earlier in Section II-C, $(a4)$ follows from the probability generating functional of the PPP [16], which states for some function $f(x)$ that $\mathbb{E}\left[\prod_{x\in\Phi}f(x)\right] = \exp(1-\lambda\int_{\mathbb{R}^2}(1-f(x))\mathrm{d}x)$, and the independence of the interference link directivity gain G_z with probability distribution $G_z = a_k$ with probability b_k. Furthermore, λ is thinned by $\mathcal{A}_L$ to capture R_z that are LOS to their serving BS. $(a5)$ follows from from computing the moment generating function of a gamma random variable g, and $(a6)$ follows from the independence of $\{R_z\}_{z\in\mathcal{Z}}$ which has been validated earlier in Section II-F and the fact that the interfering users are in LOS to their serving BS. The computation for $\mathcal{L}_{I_{LN}}(s_L)$ which denotes the Laplace transform of LOS interfering links with NLOS links to their serving BS can be obtained by following the same process such that,

$$\mathcal{L}_{I_{LN}}(s_L) = \mathbb{E}_{I_{LN}}[e^{-s_L I_{LN}}]$$
$$= \prod_{k=1}^4 e^{\left(-2\pi\lambda\mathcal{A}_N b_k\int_r^\infty e^{-\beta c}\left(1-\int_0^\infty\frac{\mathcal{F}_{R_N}(y)}{(1+s_L a_k c^{-\alpha_L} y^{\alpha_N\tau})^{N_L}}\mathrm{d}y\right)c\mathrm{d}c\right)}$$
$$= e^{-G_N(\Gamma,r)}. \tag{37}$$

Similarly, for the NLOS interfering links which are in LOS to their serving BS, $\mathcal{L}_{I_{NL}}(s_L)$ in (35) can be computed as

$$\begin{aligned}\mathcal{L}_{I_{NL}}(s_l) &= \mathbb{E}_{I_{NL}}\left[e^{-s_L I_{NL}}\right]\\ &= \mathbb{E}_{\Phi_N}\left[\exp\left\{-s_L \sum_{z:X_z\in\Phi_L\cap\bar{\mathcal{B}}(0,\zeta_L(r))\cap L} |g_z|^2 G_z D_z^{-\alpha_N} R_z^{\alpha_L\tau}\right\}\right]\\ &= \prod_{k=1}^{4} e^{\left(-2\pi\lambda\mathcal{A}_L b_k \int_{\zeta_L(r)}^{\infty}\mathcal{V}(c)\left(1-\int_0^{\infty}\frac{\mathcal{F}_{R_L}(y)}{(1+s_L a_k c^{-\alpha_N} y^{\alpha_L\tau})^{N_N}}\mathrm{d}y\right)c\mathrm{d}c\right)}\\ &= e^{-H_L(\Gamma,r)},\end{aligned} \tag{38}$$

where $\mathcal{V}(c) = 1 - e^{-\beta c}$. Furthermore, for NLOS interfering links which are NLOS to their serving BS, $\mathcal{L}_{I_{NN}}(s_L)$ in (35) can be computed as

$$\begin{aligned}\mathcal{L}_{I_{NN}}(s_L) &= \mathbb{E}_{I_{NN}}\left[e^{-s_L I_{NN}}\right]\\ &= \prod_{k=1}^{4} e^{\left(-2\pi\lambda\mathcal{A}_N b_k \int_{\zeta_L(r)}^{\infty}\mathcal{V}(c)\left(1-\int_0^{\infty}\frac{\mathcal{F}_{R_N}(y)}{(1+s_L a_k c^{-\alpha_N} y^{\alpha_N\tau})^{N_N}}\mathrm{d}y\right)c\mathrm{d}c\right)}\\ &= e^{-H_N(\Gamma,r)}\end{aligned} \tag{39}$$

Hence, we obtain (12) by substituting for $\mathcal{L}_{I_{i,j}}(s_L)$ in (35), which is further substituted into (34).

Given that the link between the desired user and the reference BS is NLOS, we can also compute the conditional probability $P_{c,N}(\Gamma)$ by following the same approach as that of $P_{c,L}(\Gamma)$. Thus we omit the detailed proof of (13) here.

Consequently, from the law of total probability, it follows that $P_c(\Gamma) = \mathcal{A}_L P_{c,L}(\Gamma) + \mathcal{A}_N P_{c,N}(\Gamma)$.

B. Proof of Theorem III.4

The coverage probability in this case can be expressed as

$$\begin{aligned}P_c(\Gamma) &= \mathcal{A}_L P_{c,L}(\Gamma) = \mathcal{A}_L \mathbb{P}\left[\mathrm{SIR} > \gamma\right]\\ &= \mathcal{A}_L \int_0^{R_B} \mathbb{P}\left[\mathrm{SIR} > \gamma\right] \overline{\mathcal{F}}_{R_L}(r)\mathrm{d}r\end{aligned}$$

where $\overline{\mathcal{F}}_{R_L}(r)$ is the simplified distribution of the distance between the reference BS and a LOS user and is obtained from (2) as $\overline{\mathcal{F}}_{R_L}(r) = \frac{2\pi\lambda r}{\mathcal{A}_L} e^{-\lambda\pi r^2}$. Hence, $P_c(\Gamma)$ can be expressed as

$$\begin{aligned}P_c(\Gamma) = \mathcal{A}_L \int_0^{R_B} &\\ \times \mathbb{P}\left[|g_0|^2 > r^{\alpha_L(1-\tau)}\Gamma I_r/(G_u^{\max}G_b^{\max})\right] &\frac{2\pi\lambda r}{\mathcal{A}_L} e^{-\lambda\pi r^2}\mathrm{d}r,\end{aligned} \tag{40}$$

where $I_r = \sum_{z:X_z\in\Phi\cap(\mathcal{B}(0,R_B)/\mathcal{B}(0,r))} |g_z|^2 D_z^{-\alpha_L} R_z^{\alpha_L\tau} P_0^L$ is the interference power given that the distance of the user served by the reference BS is $D_0 = R_0 = r$. The CCDF of the SIR at distance r can be obtained from (35) as

$$\begin{aligned}&\mathbb{P}\left[|g_0|^2 > r^{\alpha_L(1-\tau)}\Gamma I_r/(G_u^{\max}G_b^{\max}P_0^L)\right]\\ &= 1 - \mathbb{E}_{\Phi_L}\left[\left(1-\exp\left(\frac{\eta r^{\alpha_L(1-\tau)}\Gamma I_r}{G_u^{\max}G_b^{\max}}\right)\right)^N\right],\\ &= \sum_{n=1}^{N}(-1)^{n+1}\binom{N}{n}\mathbb{E}_{\Phi_L}\left[\exp\left(\frac{-\eta n r^{\alpha_L(1-\tau)}\Gamma I_r}{G_u^{\max}G_b^{\max}}\right)\right]\\ &= \sum_{n=1}^{N}(-1)^{n+1}\binom{N}{n}\mathcal{L}_{I_r}\left(\frac{\eta n r^{\alpha_L(1-\tau)}\Gamma}{G_u^{\max}G_b^{\max}}\right)\end{aligned} \tag{41}$$

where the Laplace transform of I_r is

$$\begin{aligned}\mathcal{L}_{I_r}(s) &= \mathbb{E}_{I_r}\left[e^{-sI_r}\right]\\ &= \mathbb{E}_{\Phi_L}\left[\exp\left\{-s \sum_{z:X_z\in\Phi\cap(\mathcal{B}(0,R_B)/\mathcal{B}(0,r))} |g_z|^2 G_z D_z^{-\alpha_L} R_z^{\alpha_L\tau}\right\}\right]\\ &\overset{(b1)}{=} e^{\left(-2\pi\lambda\sum_{k=1}^{4} b_k \int_r^{R_B}\left(1-\mathbb{E}_{R_z,g}\left[\exp\left\{-sga_k c^{-\alpha_L} R_z^{\alpha_L\tau}\right\}\right]\right)c\mathrm{d}c\right)}\\ &\overset{(b2)}{=} e^{\left(-2\pi\lambda\sum_{k=1}^{4} b_k \int_r^{R_B}\left(1-\mathbb{E}_{R_z}\left[\frac{1}{1+sa_k c^{-\alpha_L} R_z^{\alpha_L\tau}}\right]\right)c\mathrm{d}c\right)}\\ &\overset{(b3)}{=} e^{\left(-2\pi\lambda\sum_{k=1}^{4} b_k \int_r^{R_B}\left(1-\int_0^{\infty}\frac{\pi\lambda e^{-\lambda\pi y}}{(1+sa_k c^{-\alpha_L} y^{\frac{\alpha_L\tau}{2}})^N}\mathrm{d}y\right)c\mathrm{d}c\right)}\end{aligned} \tag{42}$$

where the dummy variable g in $(b1)$ is a normalized gamma variable with parameter N, $(a1)$ follows from the probability generating functional of the PPP [16], $(b2)$ follows from computing the moment generating function of a gamma random variable g, and $(b3)$ follows from the independence of $\{R_z\}_{z\in\mathcal{Z}}$, which has been proved earlier in Section II-F. Hence, (25) directly follows from substituting (42) into (40) and letting $s = r^{\alpha_L(1-\tau)}$.

REFERENCES

[1] J. Andrews *et al.*, "What will 5G be?" *IEEE J. Sel. Areas Commun.*, vol. 32, no. 6, pp. 1065–1082, Jun. 2014.

[2] T. Rappaport *et al.*, "Millimeter wave mobile communications for 5G cellular: It will work!" *IEEE Access*, vol. 1, pp. 335–349, 2013.

[3] Z. Pi and F. Khan, "An introduction to millimeter-wave mobile broadband systems," *IEEE Commun. Mag.*, vol. 49, no. 6, pp. 101–107, Jun. 2011.

[4] T. Baykas *et al.*, "IEEE 802.15.3c: The first IEEE wireless standard for data rates over 1 Gb/s," *IEEE Commun. Mag.*, vol. 49, no. 7, pp. 114–121, Jul. 2011.

[5] *IEEE Standard for WirelessMAN-Advanced Air Interface for Broadband Wireless Access Systems*, IEEE Std 802.16.1-2012, 2012.

[6] T. Rappaport, F. Gutierrez, E. Ben-Dor, J. Murdock, Y. Qiao, and J. Tamir, "Broadband millimeter-wave propagation measurements and models using adaptive-beam antennas for outdoor urban cellular communications," *IEEE Trans. Antennas Propag.*, vol. 61, no. 4, pp. 1850–1859, Apr. 2013.

[7] S. Rangan, T. Rappaport, and E. Erkip, "Millimeter-wave cellular wireless networks: Potentials and challenges," *Proc. IEEE*, vol. 102, no. 3, pp. 366–385, Mar. 2014.

[8] M. Akdeniz *et al.*, "Millimeter wave channel modeling and cellular capacity evaluation," *IEEE J. Sel. Areas Commun.*, vol. 32, no. 6, pp. 1164–1179, Jun. 2014.

[9] W. Roh *et al.*, "Millimeter-wave beamforming as an enabling technology for 5G cellular communications: Theoretical feasibility and prototype results," *IEEE Commun. Mag.*, vol. 52, no. 2, pp. 106–113, Feb. 2014.

[10] T. S. Rappaport, *Wireless Communications – Principles and Practice*, 2nd ed. Englewood Cliffs, NJ, USA: Prentice-Hall, 2002.

[11] A. Alejos, M. Sanchez, and I. Cuinas, "Measurement and analysis of propagation mechanisms at 40 GHz: Viability of site shielding forced by obstacles," *IEEE Trans. Veh. Technol.*, vol. 57, no. 6, pp. 3369–3380, Nov. 2008.
[12] T. Bai and R. Heath, "Coverage and rate analysis for millimeter-wave cellular networks," *IEEE Trans. Wireless Commun.*, vol. 14, no. 2, pp. 1100–1114, Feb. 2015.
[13] Z. He, S. Mao, S. Kompella, and A. Swami, "On link scheduling in dual-hop 60 GHz mmWave networks," *IEEE Trans. Veh. Technol.*, vol. 66, no. 12, pp. 11180–11192, Dec. 2017.
[14] H. Park, Y. Kim, T. Song, and S. Pack, "Multiband directional neighbor discovery in self-organized mmWave ad hoc networks," *IEEE Trans. Veh. Technol.*, vol. 64, no. 3, pp. 1143–1155, Mar. 2015.
[15] T. S. Rappapport, R. W. Heath Jr., R. C. Daniels, and J. N. Murdock, *Millimeter Wave Wireless Communications*. Englewood Cliffs, NJ, USA: Prentice-Hall, 2014.
[16] J. Andrews, F. Baccelli, and R. Ganti, "A tractable approach to coverage and rate in cellular networks," *IEEE Trans. Commun.*, vol. 59, no. 11, pp. 3122–3134, Nov. 2011.
[17] T. Novlan, H. Dhillon, and J. Andrews, "Analytical modeling of uplink cellular networks," *IEEE Trans. Wireless Commun.*, vol. 12, no. 6, pp. 2669–2679, Jun. 2013.
[18] H.-S. Jo, Y. J. Sang, P. Xia, and J. Andrews, "Heterogeneous cellular networks with flexible cell association: A comprehensive downlink SINR analysis," *IEEE Trans. Wireless Commun.*, vol. 11, no. 10, pp. 3484–3495, Oct. 2012.
[19] S. Singh, H. S. Dhillon, and J. G. Andrews, "Offloading in heterogeneous networks: Modeling, analysis, and design insights," *IEEE Trans. Wireless Commun.*, vol. 12, no. 5, pp. 2484–2497, May 2013.
[20] H. ElSawy and E. Hossain, "On stochastic geometry modeling of cellular uplink transmission with truncated channel inversion power control," *IEEE Trans. Wireless Commun.*, vol. 13, no. 8, pp. 4454–4469, Aug. 2014.
[21] M. Di Renzo, A. Guidotti, and G. Corazza, "Average rate of downlink heterogeneous cellular networks over generalized fading channels: A stochastic geometry approach," *IEEE Trans. Commun.*, vol. 61, no. 7, pp. 3050–3071, Jul. 2013.
[22] O. Onireti, A. Imran, M. Imran, and R. Tafazolli, "Energy efficient inter-frequency small cell discovery in heterogeneous networks," *IEEE Trans. Veh. Technol.*, vol. 65, no. 9, pp. 7122–7135, Sep. 2016.
[23] C. de Lima, M. Bennis, and M. Latva-aho, "Statistical analysis of self-organizing networks with biased cell association and interference avoidance," *IEEE Trans. Veh. Technol.*, vol. 62, no. 5, pp. 1950–1961, Jun. 2013.
[24] W. Bao and B. Liang, "Stochastic geometric analysis of user mobility in heterogeneous wireless networks," *IEEE J. Sel. Areas Commun.*, vol. 33, no. 10, pp. 2212–2225, Oct. 2015.
[25] T. Bai, R. Vaze, and R. Heath, "Analysis of blockage effects on urban cellular networks," *IEEE Trans. Wireless Commun.*, vol. 13, no. 9, pp. 5070–5083, Sep. 2014.
[26] M. Ding, D. López-Pérez, G. Mao, P. Wang, and Z. Lin, "Will the area spectral efficiency monotonically grow as small cells go dense?" in *Proc. IEEE Global Commun. Conf.*, San Diego, CA, USA, Dec. 2015, pp. 1–7.
[27] X. Zhang and J. Andrews, "Downlink cellular network analysis with multi-slope path loss models," *IEEE Trans. Commun.*, vol. 63, no. 5, pp. 1881–1894, May 2015.
[28] S. Singh, M. Kulkarni, A. Ghosh, and J. Andrews, "Tractable model for rate in self-backhauled millimeter wave cellular networks," *IEEE J. Sel. Areas Commun.*, vol. 33, no. 10, pp. 2196–2211, Oct. 2015.
[29] O. Onireti, A. Imran, and M. Imran, "Coverage analysis in the uplink of mmwave cellular network," in *Proc. Eur. Conf. Netw. Commun.*, Jun. 2017, pp. 1–6.
[30] J. Andrews, A. K. Gupta, and H. S. Dhillon, "A primer on cellular network analysis using stochastic geometry," Apr. 2016. [Online]. Available: http://arxiv.org/abs/1604.03183
[31] A. Simonsson and A. Furuskar, "Uplink power control in LTE – Overview and performance, subtitle: Principles and benefits of utilizing rather than compensating for SINR variations," in *IEEE 68th Veh. Technol. Conf.*, 2008, pp. 1–5.
[32] H. Alzer, "On some inequalities for the incomplete Gamma function," *Math. Comput.*,, vol. 66, no. 218, pp. 771–778, Apr. 1997.
[33] X. Yang and A. Fapojuwo, "Performance analysis of poisson cellular networks with lognormal shadowed rayleigh fading," in *Proc. IEEE Int. Conf. Commun.*, Jun. 2014, pp. 1042–1047.
[34] O. Onireti, F. Heliot, and M. Imran, "On the energy efficiency-spectral efficiency trade-off of distributed MIMO systems," *IEEE Trans. Commun.*, vol. 61, no. 9, pp. 3741–3753, Sep. 2013.
[35] R. Jain, D. Chiu, and W. Hawe, *A Quantitative Measure of Fairness and Discrimination for Resource Allocation in Shared Computer Systems*. Hudson, MA, USA: Eastern Res. Lab., Digital Equip. Corp., 1984, vol. 38.
[36] X. Yu, J. Zhang, M. Haenggi, and K. B. Letaief, "Coverage analysis for millimeter wave networks: The impact of directional antenna arrays," *IEEE J. Sel. Areas Commun.*, vol. 35, no. 7, pp. 1498–1512, Jul. 2017.

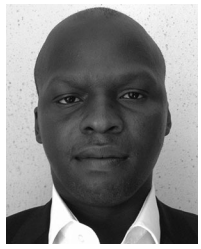

Oluwakayode Onireti (S'11–M'13) received the B.Eng. (Hons.) degree in electrical engineering from the University of Ilorin, Ilorin, Nigeria, in 2005, and the M.Sc. (Hons.) degree in mobile and satellite communications, and the Ph.D. degree in electronics engineering from the University of Surrey, Guildford, U.K., in 2009 and 2012, respectively. From 2013 to 2016, he was a Research Fellow with the 5G Innovation Centre, University of Surrey, Guildford, U.K. He is currently a Research Associate with the School of Engineering, University of Glasgow, Glasgow, U.K. He has been actively involved in projects, such as ROCKET, EARTH, Greencom, QSON, and Energy proportional EnodeB for LTE-Advanced and Beyond. He is currently involved in the DARE project, a ESPRC funded project on distributed autonomous and resilient emergency management systems. His main research interests include self-organizing cellular networks, energy efficiency, multiple-input multiple-output, and cooperative communications.

Ali Imran is the founding Director of Big Data Enabled Self-Organizing Networks Research Lab (www.bsonlab.com), University of Oklahoma. His current research interests include big data and artificial intelligence enabled wireless networks (BSON/AISON), new RAN architectures for enabling low cost human-to-human as well as IoT and D2D communications. On these topics, he has authored or coauthored more than 65 refereed journal and conference papers. He has given tutorials on these topics at several international conferences including the IEEE ICC, WF-IoT, PIMRC, WCNC, CAMAD, European Wireless, and Crowncom. He has been and is currently the Principle Investigator for several multinational research projects focused on next generation wireless networks, for which he has secured research grants of over $3 million. He is an Associate Fellow of Higher Education Academy (AFHEA), U.K.; the President of ComSoc Tulsa Chapter; the Member for Advisory Board for Special Technical Community on Big Data at IEEE Computer Society; the Board Member for ITERA, and an Associate Editor for the IEEE ACCESS. He is (co)-recipient of serval awards that include Best Paper Award IEEE CAMAD 2013, VPR Award for Outstanding International Engagement 2017, and IEEE Green ICT Best Idea Award 2017.

Muhammad Ali Imran (M'03–SM'12) received the M.Sc. (Distinction) and Ph.D. degrees from Imperial College London, London, U.K., in 2002 and 2007, respectively. He is the Vice Dean Glasgow College UESTC and Professor of communication systems with the School of Engineering, University of Glasgow. He is an Affiliate Professor at the University of Oklahoma, Norman, OK, USA, and a visiting Professor with the 5G Innovation Centre, University of Surrey, Guildford, U.K. He has more than 18 years of combined academic and industry experience, working primarily in the research areas of cellular communication systems. He has been awarded 15 patents, has authored or coauthored more than 300 journals and conference publications, and has been principal or coprincipal investigator on more than 6 million in sponsored research grants and contracts. He has supervised more than 30 successful Ph.D. graduates. He was the recipient of the award of excellence in recognition of his academic achievements, conferred by the President of Pakistan, the IEEE Comsocs Fred Ellersick Award 2014, FEPS Learning and Teaching Award 2014, and Sentinel of Science Award 2016. He was twice nominated for Tony Jeans Inspirational Teaching Award. He is a shortlisted finalist for The Wharton-QS Stars Awards 2014, QS Stars Reimagine Education Award 2016 for innovative teaching, and VCs Learning and Teaching Award in University of Surrey. He is a senior fellow of Higher Education Academy (SFHEA), U.K.